Probability in the Engineering and Informational Sciences (2026), 1–44
doi:10.1017/S0269964826100369

CAMBRIDGE UNIVERSITY PRESS

RESEARCH ARTICLE

Inspection-conditioned uncertainty and complexity in coherent systems under double periodic inspections: extropy-based measures

Reza Alizadeh Noughabi and Zohreh Pakdaman

Department of Statistics, University of Hormozgan, Iran, Islamic Republic of
Corresponding author: Reza Alizadeh Noughabi; Email: reza.alizadehn@hormozgan.ac.ir

Keywords: cumulative residual extropy; double periodic inspections; Jensen-cumulative residual extropy; order statistics; stochastic order; system signature

AMS 2000 Subject Classification: 62N05; 62F10

Reliability assessment under scheduled inspections is fundamentally an inference problem, because remaining lifetime must be evaluated conditionally on partial evidence revealed at inspection times. This paper develops a signature-based information-theoretic framework for coherent systems observed under two periodic inspections and studies the conditional residual lifetime beyond the second inspection. Uncertainty is quantified using cumulative residual extropy, yielding explicit representations and sharp comparison results that link inspection timing and system architecture to uncertainty reduction. To capture structural heterogeneity beyond uncertainty magnitude, we introduce divergence measures built from cumulative residual extropy that quantify complexity induced by coherent design under a common inspection policy. Stochastic-ordering results provide rigorous ranking tools for both inspection-conditioned lifetimes and the induced mixing structure. For statistical inference, we propose nonparametric plug-in and kernel-smoothed estimators, prove their large-sample behavior, and assess finite-sample accuracy by Monte Carlo experiments. An application to medical image intensities shows that the same two-inspection protocol produces distinct uncertainty and complexity profiles that discriminate between clinically relevant photometric transformations.

1. Introduction

In many engineered systems, uncertainty is driven not only by failure mechanisms but also by the information protocol through which system health is observed. Continuous monitoring is often infeasible; instead, systems are inspected periodically and only partial evidence is revealed at inspection times. This transforms reliability assessment into a conditional inference problem and requires tools that explicitly incorporate inspection evidence into remaining-life analysis. In particular, when the system is observed at two scheduled inspection times, the available information is updated in two stages, and the resulting residual uncertainty depends simultaneously on the component lifetime distribution, the inspection times, and the architecture of the system.

Coherent systems provide a principled language for architecture-driven reliability modeling, with deep foundations in reliability theory and ageing concepts [7, 45]. The signature representation provides a distribution-free decomposition of coherent system lifetime into order-statistic failure modes and supports architecture comparison and benchmarking [20, 46]. Because this viewpoint is inseparable from order-statistic structure, classical order-statistics theory remains central [2].

The core idea of the present paper is to combine the signature representation of coherent systems with information-theoretic uncertainty measures under a double periodic inspection protocol. In such

© The Author(s), 2026. Published by Cambridge University Press. This is an Open Access article, distributed under the terms of the Creative Commons Attribution licence (http://creativecommons.org/licenses/by/4.0), which permits unrestricted re-use, distribution and reproduction, provided the original article is properly cited.

Downloaded from https://www.cambridge.org/core. UNIVERSIDAD AUTONOMA METROPOLITANA, on 17 Nov 2026 at 01:28:28, subject to the Cambridge Core terms of use, available at https://www.cambridge.org/core/terms. https://doi.org/10.1017/S0269964826100369

a setting, one is not merely interested in the unconditional lifetime of the system, but rather in the remaining lifetime after incorporating the evidence revealed by two inspection times. This evidence changes the conditional distribution of the system lifetime in a structure-dependent way. Therefore, a suitable uncertainty measure should be able to reflect both the inspection-conditioned nature of the lifetime information and the structural heterogeneity induced by the coherent design.

This paper focuses on a canonical and practically important scheme: two inspections at ordered times $0 < t_1 < t_2$ under the event $t_1 < X_{j:n} < t_2 < T(n)$, which encodes the operational narrative that fewer than j component failures occur by t_1, at least j failures occur by t_2, and the system is still alive at t_2. Under this evidence, the object of interest becomes the conditional residual lifetime beyond t_2. The system lifetime is modeled by an absolutely continuous distribution, and all information-theoretic measures are developed in continuous time. The periodic inspections at t_1 and t_2 provide the conditioning events, but the analysis itself is conducted within a continuous-time framework. A key structural advantage of the double periodic inspection model is that the conditional survival law admits an explicit finite-mixture representation in terms of conditional order-statistic residual survivals, with mixing weights governed jointly by inspection timing and coherent architecture through the signature. To clarify the operational meaning of double inspections and conditional residual lifetime, we note two representative settings.

(1) Consider a backup power unit composed of multiple battery cells arranged in a coherent architecture. The unit is inspected at scheduled checkpoints $t_1 < t_2$. A typical outcome is that fewer than j cells have failed by t_1, while by t_2 at least j failures have occurred but the system remains operational. Under this scenario, the remaining service time beyond t_2 depends sharply on the inspection-induced restriction on unobserved failure configurations, directly impacting replacement scheduling and redundancy planning.
(2) Flight-control architectures rely on redundancy and periodic diagnostics. Even when partial failures are detected at an early inspection time, the system may remain functional at a later inspection. Engineers must quantify how long the system is expected to continue operating given the inspection evidence, because this conditional assessment informs certification margins and fault-tolerant design.

These examples illustrate why a double periodic inspection protocol is not simply a minor extension of a single-inspection model. The first inspection provides partial survival information, whereas the second inspection further restricts the set of admissible component-failure configurations. Consequently, the resulting conditional residual lifetime is governed by an interaction between ageing, inspection timing, and system structure.

For clarity, Table 1 summarizes the principal notation used throughout the manuscript.

Let a coherent system of order n consist of independent and identically distributed (IID) components $X_1, \ldots, X_n$ with common absolutely continuous CDF F. Let $T(n)$ denote the system lifetime. In this work, we focus on coherent systems with signature vectors of the form

$$\boldsymbol{s} = (0, \ldots, 0, s_i, s_{i+1}, \ldots, s_n), \qquad i = 2, \ldots, n,$$

so that the system cannot fail before the ith component failure. Assume the system is inspected at two times $0 < t_1 < t_2$. One inspection scenario of fundamental importance studied in [13] is the event

$$t_1 < X_{j:n} < t_2 < T(n), \qquad j = 1, \ldots, i-1,$$

meaning that by time t_1 fewer than j component failures have occurred, by time t_2 at least j failures have occurred, and yet the system is still alive at t_2. Under this information, the conditional residual lifetime of the system beyond t_2 is

$$T_{j,n}(t_1, t_2) = T(n) - t_2 \,\Big|\, \big(t_1 < X_{j:n} < t_2 < T(n)\big).$$

Downloaded from https://www.cambridge.org/core. UNIVERSIDAD AUTONOMA METROPOLITANA, on 17 Nov 2026 at 01:28:28, subject to the Cambridge Core terms of use, available at https://www.cambridge.org/core/terms. https://doi.org/10.1017/S0269964826100369

Table 1. *Summary of notations used throughout the manuscript.*

Notation	Description
$X_1, \ldots, X_n$	Component lifetimes
$X_{i:n}$	ith order statistic of $X_1, \ldots, X_n$
$F(\cdot)$	Cumulative distribution function (CDF) of component lifetimes
$\bar{F}(\cdot)$	Survival function (SF) of component lifetimes
$f(\cdot)$	Probability density function (PDF) of component lifetimes
$T(n)$	Lifetime of a coherent system with n components
	having lifetimes X_i, $i = 1, \ldots, n$
$\boldsymbol{s} = (s_1, \ldots, s_n)$	Signature vector,$s_k = P(T(n) = X_{k:n})$, $\sum_{k=1}^{n} s_k = 1$
$t_1 < t_2$	Two inspection times under the double periodic inspection protocol
j	Inspection index in the event $t_1 < X_{j:n} < t_2 < T(n)$
$T_{j,n}(t_1, t_2)$	Conditional residual lifetime beyond t_2 under inspection evidence
$p_k(j, t_1, t_2)$	Inspection-dependent mixing weight
$\nu_{k,j}(t_1, t_2, x)$	Conditional survival component for $X_{k:n} - t_2$
$h(t)$	Hazard rate function $f(t)/\bar{F}(t)$
$J(X)$	Extropy of X
$\xi J(X)$	Cumulative residual extropy (CRJ) of X
$JCRJ$	Jensen-CRJ divergence (JCRJ)
$R(X : Y)$	Relative CRJ of X and Y
RMSE	Root mean squared error
EW distribution	Exponentiated Weibull distribution
$\widehat{F}_N(t)$	Empirical distribution function (sample size N)
$\widehat{F}_{N,h}(t)$	Kernel-smoothed estimator of $F(t)$
$\widehat{p}_{k,N}$	Plug-in estimator of $p_k(t_1, t_2)$
$\widehat{\nu}_{k,j;N}$	Plug-in estimator of $\nu_{k,j}(t_1, t_2)$
$\widehat{p}_{k,N,h}$	Kernel-smoothed estimator of $p_k(t_1, t_2)$
$\widehat{\nu}_{k,j;N,h}$	Kernel-smoothed estimator of $\nu_{k,j}(t_1, t_2)$
N	Random sample size (distinct from system size n)
$\widehat{\xi J}_N^{\text{plug}}(t_1, t_2)$	Plug-in estimator of CRJ
$\widehat{\xi J}_N^{\text{ker}}(t_1, t_2)$	Kernel-smoothed estimator of CRJ
$\widehat{\text{JCRJ}}_N^{\text{plug}}(t_1, t_2)$	Plug-in estimator of JCRJ
$\widehat{\text{JCRJ}}_N^{\text{ker}}(t_1, t_2)$	Kernel-smoothed estimator of JCRJ

Its conditional SF is

$$\bar{F}_{T_{j,n}(t_1,t_2)}(x) = P\big(T(n) - t_2 > x \mid t_1 < X_{j:n} < t_2 < T(n)\big), \qquad x > 0.$$

A key feature of the double periodic inspection model is that this conditional SF admits an explicit finite mixture representation [13]:

$$\bar{F}_{T_{j,n}(t_1,t_2)}(x) = \sum_{k=i}^{n} p_k(j, t_1, t_2)\, \nu_{k,j}(t_1, t_2, x), \qquad x, t_1, t_2 > 0, \quad j = 1, \ldots, i-1, \tag{1}$$

where the mixture components are

$$\nu_{k,j}(t_1, t_2, x) = P\big(X_{k:n} - t_2 > x \mid t_1 < X_{j:n} < t_2 < X_{k:n}\big), \tag{2}$$

Downloaded from https://www.cambridge.org/core. UNIVERSIDAD AUTONOMA METROPOLITANA, on 17 Nov 2026 at 01:28:28, subject to the Cambridge Core terms of use , available at https://www.cambridge.org/core/terms. https://doi.org/10.1017/S0269964826100369

and the inspection-dependent mixing weights are

$$p_k(j,t_1,t_2) = P\big(T(n) = X_{k:n} \mid t_1 < X_{j:n} < t_2 < T(n)\big), \qquad k = i,\dots,n. \tag{3}$$

Moreover, the weights $p_k(j,t_1,t_2)$ have the explicit signature-based form

$$p_k(j,t_1,t_2) = \frac{s_k \sum_{r=0}^{k-j-1}\sum_{l=0}^{j-1}\binom{n}{j+r}\binom{j+r}{l}F(t_1)^l\big(F(t_2)-F(t_1)\big)^{j+r-l}\big(1-F(t_2)\big)^{n-j-r}}{\sum_{k=i}^{n} s_k \sum_{r=0}^{k-j-1}\sum_{l=0}^{j-1}\binom{n}{j+r}\binom{j+r}{l}F(t_1)^l\big(F(t_2)-F(t_1)\big)^{j+r-l}\big(1-F(t_2)\big)^{n-j-r}}. \tag{4}$$

The conditional component $\nu_{k,j}(t_1,t_2,x)$ in (2) can be written explicitly as

$$\nu_{k,j}(t_1,t_2,x) = \frac{\sum_{r=0}^{k-j-1}\sum_{l=0}^{j-1}\binom{n}{j+r}\binom{j+r}{l}(\phi(t_1))^l(F(x\mid t_1,t_2))^{j+r-l}(1-F(x\mid t_1,t_2))^{n-j-r}}{\sum_{r=0}^{k-j-1}\sum_{l=0}^{j-1}\binom{n}{j+r}\binom{j+r}{l}(\phi(t_1))^l(F(0\mid t_1,t_2))^{j+r-l}(1-F(0\mid t_1,t_2))^{n-j-r}}, \tag{5}$$

where

$$\phi(t_1) = \frac{F(t_1)}{1-F(t_1)}, \qquad F(x\mid t_1,t_2) = \frac{F(t_2+x)-F(t_1)}{1-F(t_1)}.$$

Representation (1) shows that, under double periodic inspection, the system residual life beyond t_2 is a finite mixture of conditional residual lifetimes of order statistics, with weights governed jointly by the system architecture, through the signature $\boldsymbol{s}$, and the inspection times (t_1,t_2). This mixture structure provides a natural and analytically tractable probabilistic basis for developing information-theoretic uncertainty measures.

In the realm of information theory, entropy is a fundamental measure of uncertainty introduced by [49]. As a dual counterpart, extropy was proposed by [21]. For a nonnegative random variable X with PDF $f(x)$, extropy is defined by

$$J(X) = -\frac{1}{2}\int_0^\infty f^2(x)\,dx.$$

A cumulative residual counterpart tailored to SFs is the CRJ, defined as

$$\xi J(X) = -\frac{1}{2}\int_0^\infty \bar{F}_X^2(x)\,dx, \tag{6}$$

where $\bar{F}_X$ is the SF of X. Because CRJ is formulated directly in terms of the SF, it is particularly natural for reliability analysis, where tail behavior and remaining-life uncertainty are central. In the present inspection-conditioned setting, the SF entering (6) is precisely the conditional SF in (1). Hence, CRJ provides a direct way to quantify the uncertainty remaining after the two inspection times have been taken into account.

A broad literature studies system-level residual life, mean residual life, and related quantities for coherent structures, as well as related mean residual life functionals [4]. Early work on parallel and k-out-of-n systems established systematic residual-life characterizations [3, 23]. Extensions to general coherent systems and refined structural properties have been developed in multiple directions [6, 22, 24, 29]. Residual-life functionals for systems with series/parallel structure and live components have been studied from both modeling and ordering perspectives [10, 14, 52]. Reliability and mean residual life

Downloaded from https://www.cambridge.org/core. UNIVERSIDAD AUTONOMA METROPOLITANA, on 17 Nov 2026 at 01:28:28, subject to the Cambridge Core terms of use, available at https://www.cambridge.org/core/terms. https://doi.org/10.1017/S0269964826100369

under active redundancy and specific dependence models have also been addressed [8, 51]. More recent studies have further enriched this line of research by considering coherent systems with non-identically distributed component lifetimes [17].

Inspection and monitoring schemes generate conditional lifetimes that differ qualitatively from unconditional residual life, because the observed inspection evidence restricts the set of possible failure histories. Mean past and mean residual life under double and multi monitoring have been developed, including k-out-of-n and $(n - k + 1)$-out-of-n settings [43, 54]. Residual lifetime under double monitoring for consecutive structures and coherent systems has been studied in detail [11, 13, 15, 42], and mixture representations and preservation results under double monitoring have been established [12, 53]. Inactivity times and inspection-driven behavior for dependent components under periodical inspection schemes further broaden this picture [30, 33, 50]. Extensions involving copula properties and distribution-free comparisons also contribute important comparison tools [27, 28, 32, 33].

System signatures and their extensions provide a central bridge between architecture and stochastic behavior [20, 25, 46]. Comparisons among coherent systems with dependent components using signatures and copulas have been developed [30, 31], and exchangeability-based bounds further support distribution-free analysis [34]. Complementary probabilistic tools such as spacing-based stochastic properties also inform related order-statistic arguments [26]. In the present paper, the signature is used not only as a distribution-free structural descriptor, but also as the mechanism through which the coherent architecture enters the inspection-conditioned residual lifetime mixture.

The present work is positioned at the intersection of three research streams. The first stream concerns signature-based analysis of coherent systems, where the system lifetime is represented as a mixture of ordered component lifetimes and structural comparisons can be performed separately from the baseline component distribution. The second stream is inspection-based reliability analysis, in which the available lifetime information is updated at predetermined inspection times and residual performance is assessed conditionally on survival evidence. The third stream consists of information-theoretic uncertainty measures, particularly extropy-type functionals, which provide complementary descriptions of uncertainty in nonnegative lifetime models. By integrating these three streams, the proposed framework provides a structure-aware and inspection-conditioned quantification of uncertainty and complexity for coherent systems.

Despite the maturity of inspection-conditioned residual-life theory, the information-theoretic quantification of residual uncertainty under double periodic inspections remains comparatively underdeveloped. Existing entropy and extropy-based tools have provided powerful ways to measure uncertainty, heterogeneity, and complexity in lifetime and system-reliability settings, including Jensen-type constructions and survival-based divergence measures [5, 16, 44]. Recent developments have further connected CRJ and extropy-type indices to coherent and mixed systems, relative and divergence-based extropy measures, failure extropy, and residual-lifetime complexity [1, 9, 19, 35–41, 47]. However, to the best of our knowledge, no systematic framework has yet combined system signatures, double periodic inspection information, and CRJ to quantify the conditional uncertainty of coherent systems. Moreover, Jensen-type CRJ-based measures for comparing the structural complexity induced by different coherent designs under common double-inspection evidence have not been developed. This gap motivates the present study.

The originality of the proposed approach lies in treating the double periodic inspection evidence as part of the information structure of the reliability problem and then embedding this conditional structure into CRJ-based uncertainty and Jensen-CRJ-based complexity measures. The resulting indices do not merely summarize the baseline component lifetime distribution; rather, they quantify the uncertainty and heterogeneity that remain after the inspection evidence and the coherent architecture have jointly shaped the conditional residual lifetime law.

This paper develops a signature-based information-theoretic framework for coherent systems under double periodic inspections with the following integrated components.

Downloaded from https://www.cambridge.org/core. UNIVERSIDAD AUTONOMA METROPOLITANA, on 17 Nov 2026 at 01:28:28, subject to the Cambridge Core terms of use , available at https://www.cambridge.org/core/terms. https://doi.org/10.1017/S0269964826100369

- We introduce an inspection-conditioned CRJ framework for coherent systems under double periodic inspections. The proposed measure quantifies the cumulative residual uncertainty of the system lifetime after incorporating the information revealed by two scheduled inspection times.
- Using the system signature representation, we derive finite-mixture expressions for the proposed CRJ measure. These expressions separate the role of the component lifetime distribution from the role of the coherent system structure and therefore provide a tractable tool for comparing different designs under the same inspection protocol.
- We develop Jensen-type and relative CRJ-based divergence measures, with emphasis on the Jensen-CRJ (JCRJ), to quantify architecture-driven complexity and heterogeneity induced by different coherent designs under common inspection evidence.
- We establish stochastic-ordering results that allow coherent systems to be ranked in terms of inspection-conditioned CRJ and JCRJ. These results provide theoretical support for identifying structures with larger or smaller residual uncertainty and complexity, building on conditional lifetime-ordering theory and the stochastic-orders toolkit [18, 48].
- Beyond theory, we propose nonparametric plug-in and kernel-smoothed estimators for the CRJ and JCRJ measures under double periodic inspections, study their large-sample behavior, and assess their finite-sample performance via Monte Carlo experiments under several lifetime distributions.
- To demonstrate practical applicability beyond classical reliability settings, we present a medical image analysis example. In this illustration, normalized image intensities are mapped to the same two-inspection mechanism, and the resulting CRJ and JCRJ profiles are used as methodological summaries of uncertainty and structural heterogeneity under a fixed inspection protocol.

The remainder of the paper is organized as follows. Section 2 develops CRJ for inspection-conditioned residual lifetimes and establishes stochastic-order tools for theoretical ranking. Section 3 introduces divergence measures of structural complexity. Section 4 presents nonparametric estimation and evaluates performance via Monte Carlo studies for both the inspection-conditioned uncertainty index CRJ and the corresponding complexity index JCRJ. Section 5 illustrates the proposed methodology through a medical imaging application under the same two-inspection protocol. Section 6 concludes.

2. CRJ of conditional residual lifetime of coherent systems under double regularly checking

Let $X_1, \ldots, X_n$ denote the lifetimes of the components of a coherent system of order n, with system lifetime $T(n)$ and signature vector $\boldsymbol{s} = (0, \ldots, 0, s_i, s_{i+1}, \ldots, s_n)$, where $i = 2, \ldots, n$. Throughout this section, we focus on the double regularly checking scenario $t_1 < X_{j:n} < t_2 < T(n)$, for $j = 1, \ldots, i-1$, introduced in Section 1. Under this inspection information, the conditional residual lifetime of interest is $T_{j,n}(t_1, t_2)$ with conditional SF $F_{T_{j,n}(t_1,t_2)}(x)$ given in (1). The CRJ of the conditional residual lifetime $T_{j,n}(t_1, t_2)$ is defined as

$$\begin{aligned} \xi J\big(T_{j,n}(t_1,t_2)\big) &= -\frac{1}{2}\int_0^\infty \left(\bar{F}_{T_{j,n}(t_1,t_2)}(x)\right)^2 dx \\ &= -\frac{1}{2}\int_0^\infty \left(\sum_{k=i}^{n} p_k(j,t_1,t_2)\, \nu_{k,j}(t_1,t_2,x)\right)^2 dx. \end{aligned} \tag{7}$$

Using the explicit forms of the mixing weights $p_k(j, t_1, t_2)$ and the conditional components $\nu_{k,j}(t_1, t_2, x)$ given in (4) and (5), respectively, Eq. (7) admits an explicit integral representation depending on the system signature and inspection times (t_1, t_2). In particular, the CRJ is governed by the inspection-dependent probability vector

$$\boldsymbol{p}(t_1,t_2) = \big(p_1(j,t_1,t_2), \ldots, p_n(j,t_1,t_2)\big),$$

Downloaded from https://www.cambridge.org/core. UNIVERSIDAD AUTONOMA METROPOLITANA, on 17 Nov 2026 at 01:28:28, subject to the Cambridge Core terms of use, available at https://www.cambridge.org/core/terms. https://doi.org/10.1017/S0269964826100369

so that $\sum_{k=i}^{n} p_k(j,t_1,t_2) = 1$, which can be interpreted as a conditional signature of the system under the inspection information $t_1 < X_{j:n} < t_2 < T$. Note that the vector $\boldsymbol{p}(t_1,t_2)$ depends on j through its components $p_k(j,t_1,t_2)$ and has dimension n (the system size). Throughout the text, this dependence is implicit in the notation. Representation (7) shows that, under double regularly checking, the CRJ of the system residual lifetime beyond t_2 is a weighted functional of the conditional survival components $\nu_{k,j}(t_1,t_2,x)$. The weights $p_k(j,t_1,t_2)$ jointly reflect the effects of system architecture and inspection timing on uncertainty accumulation. As a result, CRJ provides an informative measure for assessing the uncertainty of system performance under partial inspection information and allows coherent systems with similar unconditional behavior to be distinguished through their conditional residual structures.

Example 1. Consider a coherent system of order $n = 4$ with IID component lifetimes $X_1,\ldots,X_4$ and system lifetime $T(4)$. We focus on System 2 in Table 1, whose signature vector is $\boldsymbol{s} = \left(0, \frac{1}{3}, \frac{5}{12}, \frac{1}{4}\right)$, $i = 2$, so that the system cannot fail before the second component failure. The corresponding structure function representation is $T(4) = \max\big(X_2, \min(X_1,X_3)\big)$, which matches the "consecutive 2-out-of-3" configuration. The system is inspected at two ordered times $0 < t_1 < t_2$. We consider the fundamental double-checking scenario $t_1 < X_{1:4} < t_2 < T(4)$, meaning that no component failure is detected before t_1, at least one failure occurs by t_2, and the system is still alive at t_2. Under this inspection information, the conditional residual lifetime is $T_{1,4}(t_1,t_2) = T(4) - t_2 \,\big|\, \big(t_1 < X_{1:4} < t_2 < T(4)\big)$. Assume that each component lifetime follows a Weibull distribution with shape $\beta > 0$ and scale $\eta > 0$, with $F(x) = 1 - \exp\left\{-\left(\frac{x}{\eta}\right)^{\beta}\right\}$, $x \geq 0$. To illustrate the effect of different hazard-rate regimes (while keeping the same family), we fix $\eta = 1$ and consider three values of the shape parameter: $(\beta,\eta) \in \{(1,1), (1.6,1), (0.7,1)\}$. These correspond, respectively, to a constant hazard rate ($\beta = 1$, exponential case), an increasing hazard rate ($\beta > 1$), and a decreasing hazard rate ($\beta < 1$). Figure 1 reports the resulting six panels: three surface plots and three contour plots of $\xi J\big(T_{1,4}(t_1,t_2)\big)$, corresponding to the three Weibull parameter settings.

The contour plots provide a concise and informative visualization of how the $\xi J\big(T_{1,4}(t_1,t_2)\big)$ evolves jointly with the two inspection times t_1 and t_2 under the double regularly checking framework. Recall that the conditioning event $t_1 < X_{1:4} < t_2 < T(4)$ represents partial inspection information: no system failure is observed by time t_1, at least one component failure is detected by time t_2, while the system remains operational at t_2. Consequently, the residual lifetime beyond t_2 reflects both the structural constraints of the coherent system and the information revealed through inspections. Across all contour plots, a clear monotone pattern is observed: the CRJ values increase (i.e., move toward zero) as either t_1 or t_2 increases. This behavior is consistent with the interpretation of CRJ as a measure of uncertainty, since later inspection times correspond to stronger conditioning and hence reduced uncertainty in the residual system lifetime.

More specifically, the contour lines are typically steeper in the t_2-direction than in the t_1-direction. This indicates that the second inspection time t_2, which provides the most recent confirmation of system survival, plays a dominant role in shaping the conditional residual uncertainty. In contrast, variations in t_1 influence the CRJ more gradually, reflecting the diminishing impact of early inspection information as time progresses. The geometry of the contour lines further reveals the interaction between the two inspection times. For fixed t_2, increasing t_1 leads to higher CRJ values, indicating a reduction in uncertainty due to the restriction of admissible failure configurations prior to t_2. Similarly, for fixed t_1, increasing t_2 substantially decreases uncertainty by narrowing the set of future failure scenarios compatible with system survival beyond t_2.

From the perspective of the double inspection model, these patterns highlight a key feature: the CRJ depends not only on the elapsed time since the last inspection, but also on the width of the inspection interval (t_1,t_2). Narrower inspection intervals induce stronger conditioning and therefore lower residual uncertainty, which is reflected by higher (less negative) CRJ levels in the contour plots. Overall, the contour plots demonstrate that CRJ provides a refined characterization of conditional residual

Downloaded from https://www.cambridge.org/core. UNIVERSIDAD AUTONOMA METROPOLITANA, on 17 Nov 2026 at 01:28:28, subject to the Cambridge Core terms of use, available at https://www.cambridge.org/core/terms. https://doi.org/10.1017/S0269964826100369

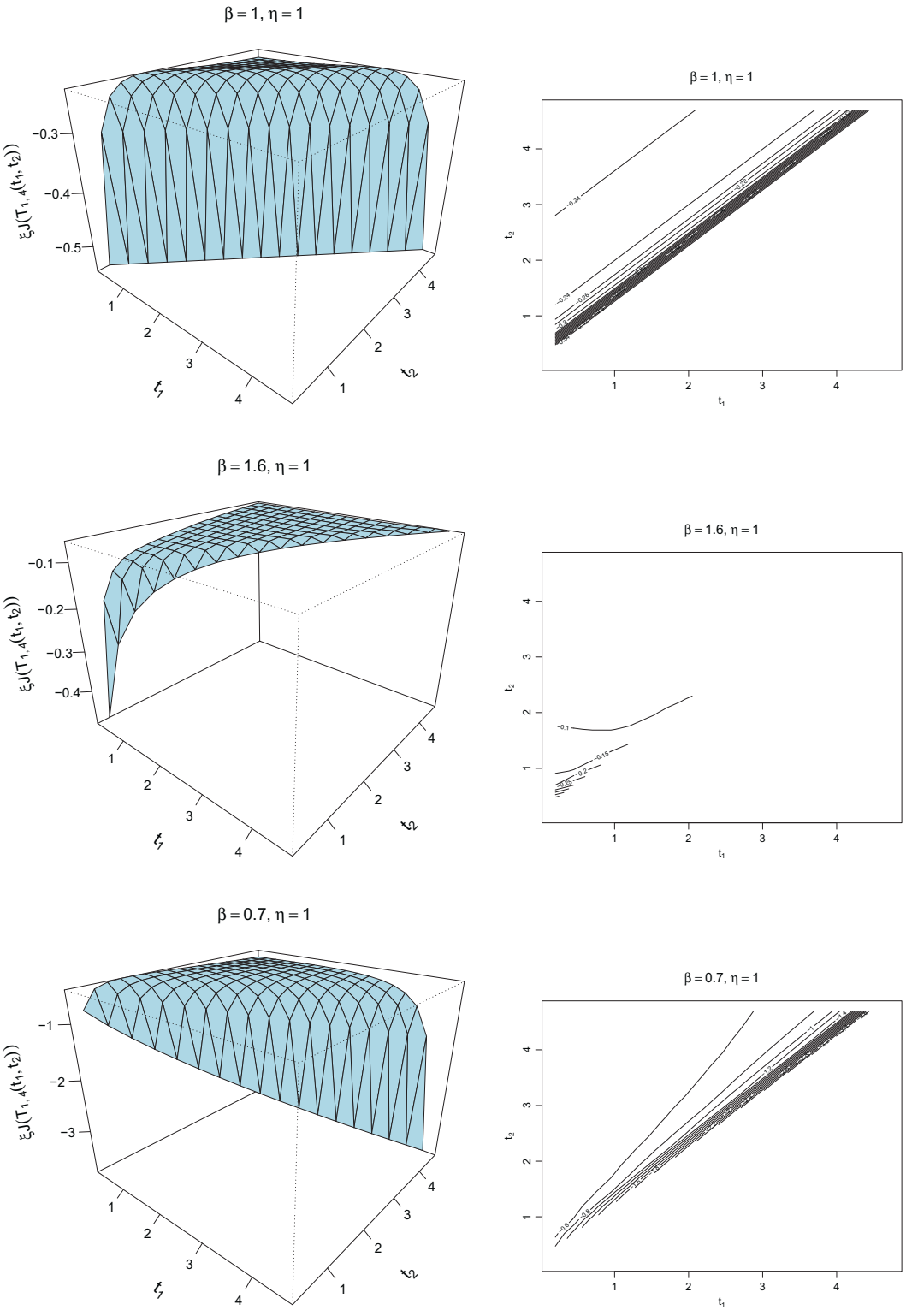


Figure 1. *Surface (left panels) and contour (right panels) plots of the CRJ* $\xi J\left(T_{1,4}(t_1,t_2)\right)$ *for System 2 under Weibull component lifetimes with different hazard-rate regimes, evaluated under double regularly checking.*

Downloaded from https://www.cambridge.org/core. UNIVERSIDAD AUTONOMA METROPOLITANA, on 17 Nov 2026 at 01:28:28, subject to the Cambridge Core terms of use, available at https://www.cambridge.org/core/terms. https://doi.org/10.1017/S0269964826100369

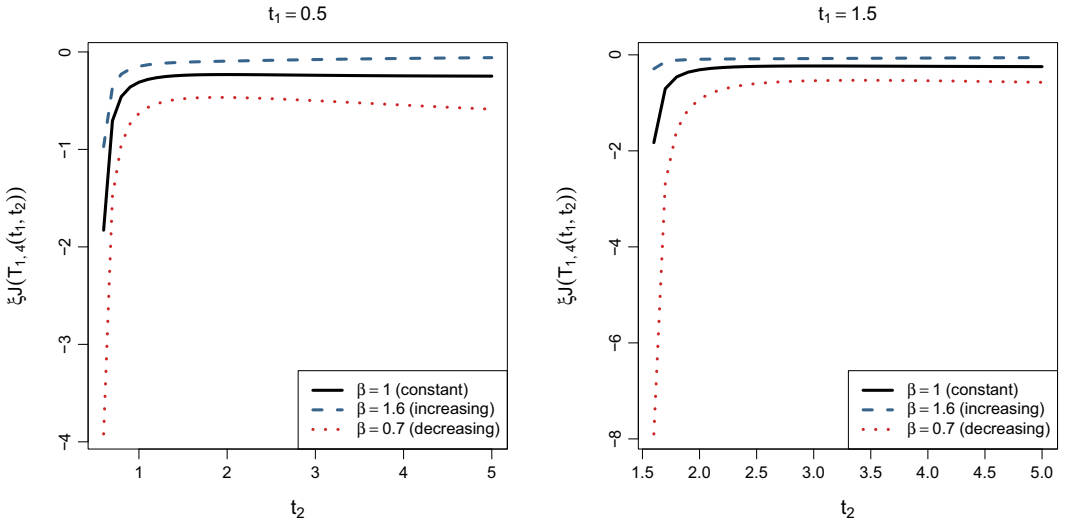


Figure 2. *CRJ* $\xi J\left(T_{1,4}(t_1, t_2)\right)$ *as a function of* t_1 *for two fixed values of* t_2*, under double regularly checking.*

uncertainty under periodic inspections. Unlike unconditional measures, it captures how inspection timing reshapes the space of admissible system trajectories, thereby revealing structural and informational effects intrinsic to coherent systems operating under double regularly checking.

A comparison of the contour plots across different hazard-rate regimes reveals that the shape of the component hazard function has a pronounced impact on the accumulation of conditional uncertainty. Under a constant hazard rate, the CRJ varies smoothly with t_1 and t_2, reflecting a balance between temporal information and system structure. In contrast, under an increasing hazard rate, later inspection times lead to a more rapid reduction in uncertainty, as the probability of component failure grows with age and survival up to t_2 conveys stronger information. Under a decreasing hazard rate, the gradual decline in failure intensity results in a slower restriction of admissible failure scenarios, yielding a more moderate increase of CRJ with respect to inspection times. These differences indicate that CRJ is sensitive not only to system architecture and inspection policy, but also to the dynamic nature of component hazard rates, thereby providing a comprehensive measure of conditional uncertainty in coherent systems under double inspection.

Figure 2 shows that, for fixed t_1, the $\xi J\left(T_{1,4}(t_1, t_2)\right)$ approaches a stable level as t_2 increases, regardless of the hazard-rate regime. This indicates that, beyond a sufficiently large second inspection time, additional survival information does not significantly reduce uncertainty. The convergence is faster under increasing hazard rates and slower under decreasing hazard rates, reflecting the differing informational content of late-life survival across regimes.

To further assess the performance of the CRJ under the double regularly checking framework, we next consider component lifetime models with a bathtub-shaped hazard rate. Such models are fundamental in reliability engineering, as they capture early-life failures, a period of stable operation, and eventual wear-out. The following example investigates the CRJ behavior of a coherent system under double regularly checking when component lifetimes exhibit a bathtub-shaped hazard rate.

Example 2. Consider a coherent system of order four with IID component lifetimes $X_1, \ldots, X_4$. We focus on System 3 in Table 1, whose signature vector is $\boldsymbol{s} = \left(0, \frac{1}{2}, \frac{1}{4}, \frac{1}{4}\right)$, The corresponding structure function representation of the system lifetime is $T(4) = \max\left(X_1, \min(X_2, X_3, X_4)\right)$. Each component

Downloaded from https://www.cambridge.org/core. UNIVERSIDAD AUTONOMA METROPOLITANA, on 17 Nov 2026 at 01:28:28, subject to the Cambridge Core terms of use, available at https://www.cambridge.org/core/terms. https://doi.org/10.1017/S0269964826100369

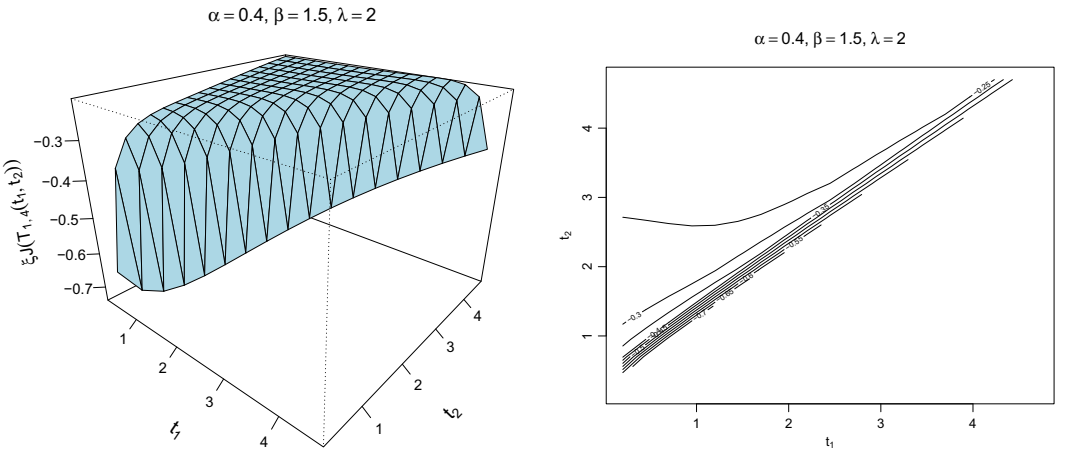


Figure 3. *Surface (left) and contour (right) plots of the* $\xi J\big(T_{1,4}(t_1,t_2)\big)$ *for the coherent system* $T(4) = \max\big(X_1, \min(X_2, X_3, X_4)\big)$*, under EW component lifetimes, evaluated within the double regularly checking framework.*

lifetime is assumed to follow an EW distribution with CDF $G(y) = \left(1 - \exp\left\{-\left(\frac{y}{\lambda}\right)^{\beta}\right\}\right)^{\alpha}$, $y > 0$. where $\alpha > 0$, $\beta > 0$, and $\lambda > 0$ are shape and scale parameters. The EW family is particularly suitable in reliability analysis due to its ability to generate non-monotone hazard-rate patterns, including bathtub-shaped behavior. The system is inspected at two ordered times $0 < t_1 < t_2$, and we consider the double regularly checking scenario $t_1 < X_{1:4} < t_2 < T(4)$. Under this inspection information, the conditional residual lifetime beyond t_2 is defined by $T_{1,4}(t_1,t_2) = T(4) - t_2 \,\big|\, \big(t_1 < X_{1:4} < t_2 < T(4)\big)$. In the numerical illustrations below, we consider a set of EW parameters that yield bathtub-shaped hazard rates as $(\alpha, \beta, \lambda) = (0.4, 1.5, 2)$. Surface and contour plots of the resulting CRJ are used to examine how early-life failures and wear-out effects interact with inspection timing and system structure under double regularly checking.

As shown in Figure 3, the surface and contour plots indicate that $\xi J\big(T_{1,4}(t_1,t_2)\big)$ exhibits a pronounced nonlinear dependence on the inspection times (t_1, t_2) under a bathtub-shaped hazard rate. Early inspections are associated with higher uncertainty due to the persistence of infant-failure effects, whereas inspections conducted in the wear-out phase lead to a stabilized CRJ surface. The curved contour lines further reveal a strong interaction between t_1 and t_2, emphasizing the critical role of inspection timing in uncertainty reduction for systems governed by nonmonotone hazard mechanisms.

Figure 4 complements the surface/contour visualization by isolating the marginal impact of each inspection time on the conditional residual uncertainty. In the left panel, increasing t_2 (with t_1 fixed) typically drives $\xi J\big(T_{1,4}(t_1,t_2)\big)$ upward toward zero, reflecting that a later confirmation of system survival at the second inspection imposes stronger conditioning and hence reduces uncertainty in the remaining lifetime beyond t_2. In the right panel, varying t_1 (with t_2 fixed) produces a milder but systematic effect: as t_1 increases, the admissible failure histories within (t_1, t_2) become more constrained, leading again to less negative CRJ levels. The separation between the two curves in each panel shows how early versus later inspection information contributes differently to uncertainty reduction, consistent with the double-inspection mechanism that couples the inspection window length $(t_2 - t_1)$ with the system's coherent structure.

By employing Eq. (7), the CRJ associated with conditional residual lifetimes under double regularly checking can be systematically evaluated, allowing for meaningful comparisons across different coherent system structures. This formulation explicitly incorporates the inspection-induced conditioning and the system signature into the uncertainty assessment. To support such comparisons, several stochastic

Downloaded from https://www.cambridge.org/core. UNIVERSIDAD AUTONOMA METROPOLITANA, on 17 Nov 2026 at 01:28:28, subject to the Cambridge Core terms of use, available at https://www.cambridge.org/core/terms. https://doi.org/10.1017/S0269964826100369

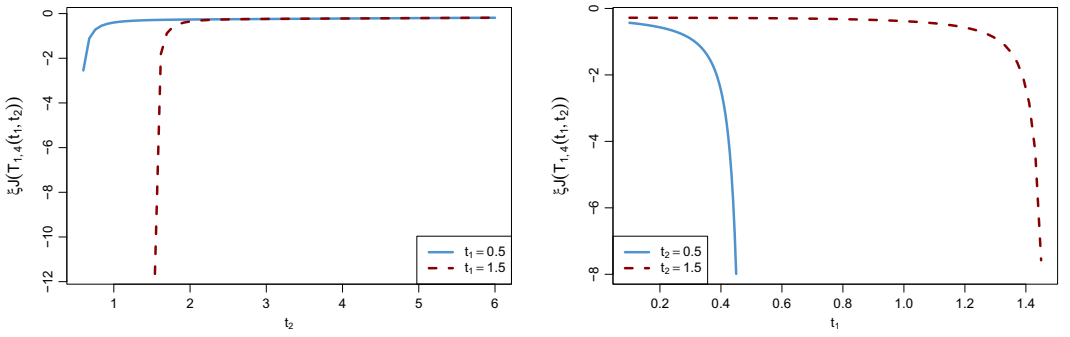


Figure 4. *Slice plots of $\xi J\big(T_{1,4}(t_1,t_2)\big)$ under double regularly checking: (left) as a function of t_2 for two fixed values of t_1, and (right) as a function of t_1 for two fixed values of t_2.*

orderings are recalled, which provide the theoretical basis for ranking conditional residual lifetime distributions and their CRJ values. These orderings, as developed in [48] and further discussed in [48], underpin the comparative results established in this section.

Definition 1. ***(Stochastic orders)*** *Let X and Y be two random variables with CDFs F and G and PDFs f and g, respectively. Then X is said to be smaller than Y in the sense of:*

(i) usual stochastic order (denoted by $X \leqslant_{st} Y$ or $F \leqslant_{st} G$) if $\bar{F}(x) \leq \bar{G}(x)$ for all x;

(ii) hazard rate order (denoted by $X \leqslant_{hr} Y$ or $F \leqslant_{hr} G$) if $\dfrac{\bar{G}(x)}{\bar{F}(x)}$ is increasing in x.

(iii) disperse order (denoted by $X \leqslant_{disp} Y$ or $F \leqslant_{disp} G$) if $g(G^{-1}(v)) \leq f(F^{-1}(v))$ for all $0 < v < 1$.

Also, let $\boldsymbol{p}$ and $\boldsymbol{q}$ be two discrete distributions on the integers $\{1, ..., n\}$. Then, it is said that (see, for example, Kochar et al. 1999)

(iv) $\boldsymbol{p} \leqslant_{st} \boldsymbol{q}$ if and only if $\sum_{i=j}^{n} p_i \leq \sum_{i=j}^{n} q_i$, for $j = 1, \cdots, n$.

(v) $\boldsymbol{p} \leqslant_{hr} \boldsymbol{q}$ if and only if $\sum_{i=j}^{n} p_i \Big/ \sum_{i=j}^{n} q_i$ is decreasing in j, for $j = 1, \cdots, n$.

(vi) $\boldsymbol{p} \leqslant_{lr} \boldsymbol{q}$ if and only if p_i/q_i is decreasing in i, for $i = 1, \cdots, n$ when $p_i, q_i > 0$.

In what follows, we formalize the conditional residual lifetime of a coherent system under double regularly checking through the model

$$\mathcal{M}_{T_{j,n}(t_1,t_2),\, \nu_{k,j}(t_1,t_2,\cdot),\boldsymbol{p}(t_1,t_2),T(n),\boldsymbol{s},\boldsymbol{X},F} = \big\{T_{j,n}(t_1,t_2),\ \nu_{k,j}(t_1,t_2,\cdot),\ \boldsymbol{p}(t_1,t_2),$$
$$T(n) = \phi(X_1,\ldots,X_n),\ \boldsymbol{s} = (s_1,\ldots,s_n),\ \boldsymbol{X} = (X_1,\ldots,X_n),\ F\big\},$$

where X_i for $i = 1, ..., n$ are IID component lifetimes with common CDF F. Here, $T_{j,n}(t_1,t_2) = T(n) - t_2 \mid (t_1 < X_{j:n} < t_2 < T(n))$ denotes the conditional residual lifetime beyond the second inspection time, and $\boldsymbol{p}(t_1,t_2)$ is the inspection dependent probability vector defined in (4). Within this framework, the CRJ $\xi J\big(T_{j,n}(t_1,t_2)\big)$ in (7) provides a concise measure of conditional residual uncertainty. In the sequel, we compare the CRJ of coherent systems by exploiting stochastic orderings with respect to the inspection times (t_1,t_2) and the induced vectors $\boldsymbol{p}(t_1,t_2)$, thereby characterizing how system structure and inspection timing jointly govern conditional uncertainty.

We next establish stochastic-ordering comparisons for the conditional residual lifetime under double regularly checking. The key driver of these comparisons is the inspection-dependent mixing vector $\boldsymbol{p}(t_1,t_2)$, which acts as a conditional signature under the event $t_1 < X_{j:n} < t_2 < T(n)$.

Theorem 1 *Consider* $\mathcal{M}^{X}_{T^{X}_{j,n}(t_1,t_2),\, \nu^{X}_{k,j}(t_1,t_2,\cdot),\boldsymbol{p}^{X}(t_1,t_2),T^{X}(n),\boldsymbol{s}^{X},\boldsymbol{X},F}$ *and*

Downloaded from https://www.cambridge.org/core. UNIVERSIDAD AUTONOMA METROPOLITANA, on 17 Nov 2026 at 01:28:28, subject to the Cambridge Core terms of use, available at https://www.cambridge.org/core/terms. https://doi.org/10.1017/S0269964826100369

$\mathcal{M}^{Y}_{T^{Y}_{j,n}(t_1,t_2),\nu^{Y}_{k,j}(t_1,t_2,\cdot),\boldsymbol{p}^{Y}(t_1,t_2),T^{Y}(n),\boldsymbol{s}^{Y},\boldsymbol{Y},F}$ *as the model structures representing conditional residual lifetime of coherent systems operating under double periodic inspection.*

(i) If $\boldsymbol{p}^{X}(t_1,t_2) \leq_{st} \boldsymbol{p}^{Y}(t_1,t_2)$, *then* $\xi J\left(T^{X}_{j,n}(t_1,t_2)\right) \geq \xi J\left(T^{Y}_{j,n}(t_1,t_2)\right)$.

(ii) If $\boldsymbol{p}^{X}(t_1,t_2) \leq_{hr} \boldsymbol{p}^{Y}(t_1,t_2)$, *then* $\xi J\left(T^{X}_{j,n}(t_1,t_2)\right) \geq \xi J\left(T^{Y}_{j,n}(t_1,t_2)\right)$.

(iii) If $\boldsymbol{p}^{X}(t_1,t_2) \leq_{lr} \boldsymbol{p}^{Y}(t_1,t_2)$, *then* $\xi J\left(T^{X}_{j,n}(t_1,t_2)\right) \geq \xi J\left(T^{Y}_{j,n}(t_1,t_2)\right)$.

Proof. These conclusions can be directly inferred from Theorem 2.5 in [13], which provides the formal foundation for this result. □

We now provide a numerical illustration of Theorem 1.

Example 3. Consider two coherent systems of order $n = 4$ with IID component lifetimes $X_1, \ldots, X_4$ following a Weibull distribution with CDF $F(x) = 1-\exp\left\{-\left(\frac{x}{\eta}\right)^{\beta}\right\}$, $x \geq 0$, where $\beta \in (0,1)$ and $\eta > 0$, so that the component hazard rate is decreasing. We work under the double regularly checking condition $t_1 < X_{j:4} < t_2 < T$, and take $j = 2$. Let System X and System Y have signature vectors $\boldsymbol{s}^{X} = \left(0, 0, \frac{1}{2}, \frac{1}{2}\right)$, $\boldsymbol{s}^{Y} = (0,0,0,1)$, respectively. The second system corresponds to the 4-parallel structure, while the first allocates equal signature weight to the third and fourth order statistics. For $j = 2$, the inspection-dependent mixing vectors are $\boldsymbol{p}^{X}(t_1,t_2) = \left(0, 0, p^{X}_{3}(t_1,t_2), p^{X}_{4}(t_1,t_2)\right)$, $\boldsymbol{p}^{Y}(t_1,t_2) = (0,0,0,1)$, where, from (4),

$$p^{X}_{3}(t_1,t_2) = \frac{A_3(t_1,t_2)}{A_3(t_1,t_2)+A_4(t_1,t_2)}, \qquad p^{X}_{4}(t_1,t_2) = \frac{A_4(t_1,t_2)}{A_3(t_1,t_2)+A_4(t_1,t_2)},$$

with

$$A_3(t_1,t_2) = 6\big(1-F(t_2)\big)^2\Big(\Delta^2 + 2F(t_1)\Delta\Big),$$

$$A_4(t_1,t_2) = 6\big(1-F(t_2)\big)^2\Big(\Delta^2 + 2F(t_1)\Delta\Big) + 4\big(1-F(t_2)\big)\Big(\Delta^3 + 3F(t_1)\Delta^2\Big), \qquad \Delta := F(t_2) - F(t_1).$$

Since for all $0 < t_1 < t_2$ we have

$$\sum_{m=4}^{4} p^{X}_{m}(t_1,t_2) = p^{X}_{4}(t_1,t_2) \leq 1 = \sum_{m=4}^{4} p^{Y}_{m}(t_1,t_2),$$

and for $r = 1, 2, 3$,

$$\sum_{m=r}^{4} p^{X}_{m}(t_1,t_2) = 1 = \sum_{m=r}^{4} p^{Y}_{m}(t_1,t_2),$$

it follows that $\boldsymbol{p}^{X}(t_1,t_2) \leq_{st} \boldsymbol{p}^{Y}(t_1,t_2)$, for all $0 < t_1 < t_2$. Hence, by Theorem 1, $\xi J\left(T^{X}_{2,4}(t_1,t_2)\right) \geq \xi J\left(T^{Y}_{2,4}(t_1,t_2)\right)$, demonstrating that, under identical inspection times, System X exhibits no larger conditional residual uncertainty than System Y (see Figure 5).

Downloaded from https://www.cambridge.org/core. UNIVERSIDAD AUTONOMA METROPOLITANA, on 17 Nov 2026 at 01:28:28, subject to the Cambridge Core terms of use, available at https://www.cambridge.org/core/terms. https://doi.org/10.1017/S0269964826100369

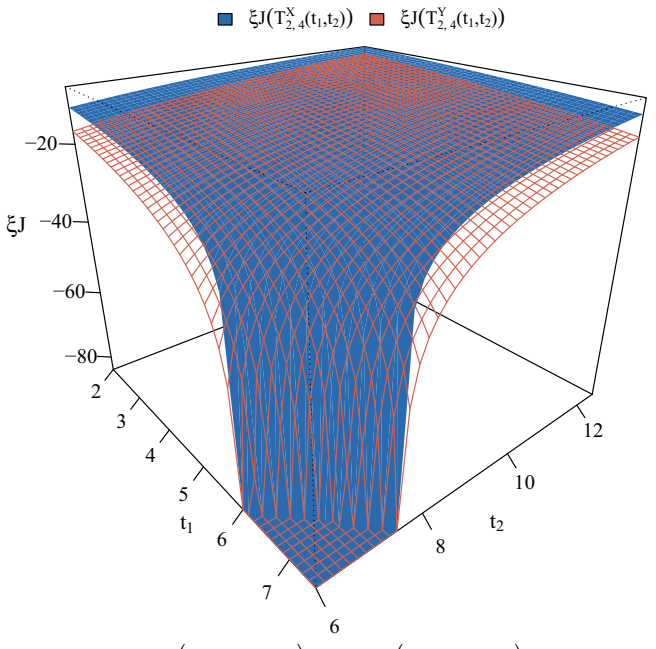


Figure 5. *Surface comparison of* $\xi J\left(T^X_{2,4}(t_1,t_2)\right)$ *and* $\xi J\left(T^Y_{2,4}(t_1,t_2)\right)$ *under double regular checking, illustrating the uniform dominance of System X over System Y.*

Theorem 2 *Consider* $\mathcal{M}^X_{T^X_{j,n}(t_1,t_2),\,\nu^X_{k,j}(t_1,t_2,\cdot),\boldsymbol{p}^X(t_1,t_2),T^X(n),\boldsymbol{s}^X,\boldsymbol{X},F}$ *and* $\mathcal{M}^Y_{T^Y_{j,n}(t_1,t_2),\,\nu^Y_{k,j}(t_1,t_2,\cdot),\boldsymbol{p}^Y(t_1,t_2),T^Y(n),\boldsymbol{s}^Y,\boldsymbol{Y},G}$ *as the model structures representing conditional residual lifetime of coherent systems operating under double periodic inspection. If* $X_1 \leq_{hr} Y_1$, *then* $\xi J\left(T^X_{j,n}(t_1,t_2)\right) \geq \xi J\left(T^Y_{j,n}(t_1,t_2)\right)$.

Proof. The conclusion follows from the stochastic-order preservation mechanism developed in Theorem 3.2 of [13], which formalizes the stability of ordering relations under inspection-induced signature mixtures. □

Example 4. Consider two coherent systems of order $n = 4$ operating under double periodic inspection at times $0 < t_1 < t_2$, and suppose that the inspection outcome corresponds to the event $t_1 < X_{1:4} < t_2 < T$, that is, no component fails before t_1, at least one component fails by t_2, and the system is still alive at t_2. Let System T^X be the coherent structure $T^X = \max\big(X_1, \min(X_2, X_3), \min(X_3, X_4)\big)$ with $\boldsymbol{s}^X = \left(0, \frac{1}{6}, \frac{7}{12}, \frac{1}{4}\right)$ and let System T^Y be the 4-parallel system $T^Y = X_{4:4} = \max(X_1, X_2, X_3, X_4)$, with $\boldsymbol{s}^Y = (0, 0, 0, 1)$. Assume that the component lifetimes in System T^X are IID Weibull with CDF $F(x) = 1 - \exp\left(-x^2\right)$, $x \geq 0$, whereas the component lifetimes in System T^Y are IID Weibull with CDF $G(x) = 1 - \exp\left(-\frac{x^2}{4}\right)$, $x \geq 0$. For a Weibull law with CDF $H(x) = 1 - \exp\{-(x/\eta)^\beta\}$, the hazard rate is $h(x) = \frac{\beta}{\eta}\left(\frac{x}{\eta}\right)^{\beta-1}$, $x > 0$. Therefore, the hazard rates corresponding to F and G are $h_X(x) = 2x$ and $h_Y(x) = \frac{x}{2}$. Hence

$$\frac{h_X(x)}{h_Y(x)} = \frac{2x}{x/2} = 4 > 1, \qquad x > 0.$$

Downloaded from https://www.cambridge.org/core. UNIVERSIDAD AUTONOMA METROPOLITANA, on 17 Nov 2026 at 01:28:28, subject to the Cambridge Core terms of use, available at https://www.cambridge.org/core/terms. https://doi.org/10.1017/S0269964826100369

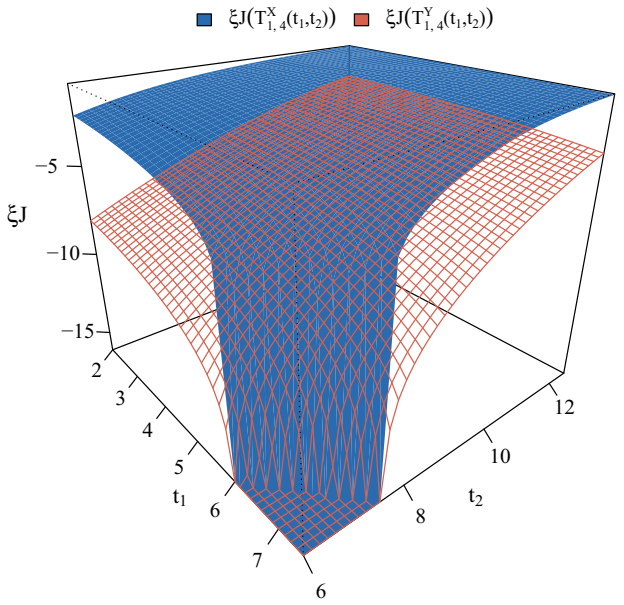


Figure 6. *Surface comparison of $\xi J\left(T^X_{1,4}(t_1,t_2)\right)$ (System 4) and $\xi J\left(T^Y_{1,4}(t_1,t_2)\right)$ (4-parallel) under double periodic inspection, illustrating the ordering induced by the hazard-rate relation $X_1 \leq_{hr} Y_1$.*

Thus $h_X(x) \geq h_Y(x)$ for all $x > 0$, which implies the hazard-rate ordering $X_1 \leq_{hr} Y_1$. Consequently, by Theorem 2, $\xi J\left(T^X_{1,4}(t_1,t_2)\right) \geq \xi J\left(T^Y_{1,4}(t_1,t_2)\right)$, $0 < t_1 < t_2$. Figure 6 visualizes this dominance over the inspection plane (t_1,t_2) by comparing the corresponding CRJ surfaces.

3. JCRJ divergence under double periodic inspection

Divergence-based functionals have long provided a principled mechanism for quantifying structural heterogeneity in coherent systems. Within the entropy framework initiated by [49], system-level complexity was compared to ordered component behavior through a Jensen–Shannon construction [5]. Replacing entropy by extropy, as introduced by [21], led to a dual Jensen–extropy formulation [44]. More recently, Chakraborty and Pradhan [9] extended this paradigm to survival analysis by grounding the divergence in CRJ, thereby introducing a Jensen-type construction based on $\xi J(\cdot)$.

The present inspection setting necessitates an explicitly conditional adaptation of this idea. Under double regularly checking, the conditional residual lifetime $T_{j,n}(t_1,t_2)$ admits the finite mixture representation (1), with inspection-dependent weights (4) and conditional survival components (5) (see [13]). This decomposition separates architectural effects, encoded through the signature vector, from inspection information, encoded through (t_1,t_2). It therefore provides a natural structural scaffold for defining a divergence that measures inspection-induced complexity.

Motivated by the JCRJ construction of [9], we define the inspection-conditioned divergence

$$\mathrm{JCRJ}_{j,n}(t_1,t_2) = \xi J\left(T_{j,n}(t_1,t_2)\right) - \sum_{k=i}^{n} p_k(j,t_1,t_2)\, \xi J\left(\nu_{k,j}(t_1,t_2,\cdot)\right), \tag{8}$$

where $\xi J(\cdot)$ is given in (6). The first term quantifies the cumulative residual uncertainty of the inspection-conditioned system lifetime, whereas the second term represents the inspection-weighted mean of the corresponding component-level conditional uncertainties.

Downloaded from https://www.cambridge.org/core. UNIVERSIDAD AUTONOMA METROPOLITANA, on 17 Nov 2026 at 01:28:28, subject to the Cambridge Core terms of use, available at https://www.cambridge.org/core/terms. https://doi.org/10.1017/S0269964826100369

To clarify the geometric content of (8), consider two nonnegative random variables U and V with SFs $\bar{F}_U$ and $\bar{F}_V$. Following the survival-based distance formulation implicit in [9], define

$$R(U : V) = \frac{1}{2} \int_0^\infty \left(\bar{F}_U(x) - \bar{F}_V(x)\right)^2 dx. \tag{9}$$

The functional $R(U : V)$ defined in (9) coincides with the relative CRJ between U and V, introduced by [9], and represents the squared L^2 separation between their SFs over $(0, \infty)$.

The following result shows that the divergence (8) coincides exactly with a signature-weighted mean of the distances (9).

Proposition 1. *For fixed $0 < t_1 < t_2$ and $j \in \{1, \dots, i-1\}$, the divergence in (8) satisfies*

$$\mathrm{JCRJ}_{j,n}(t_1, t_2) = \sum_{k=i}^{n} p_k(j, t_1, t_2)\, R\big(T_{j,n}(t_1, t_2) : \nu_{k,j}(t_1, t_2, \cdot)\big)\,. \tag{10}$$

Proof. From the mixture representation (1),

$$\bar{F}_{T_{j,n}(t_1,t_2)}(x) = \sum_{k=i}^{n} p_k(j, t_1, t_2)\, \nu_{k,j}(t_1, t_2, x), \qquad x > 0,$$

with $\sum_{k=i}^{n} p_k(j, t_1, t_2) = 1$.

Using (9) and expanding the square,

$$\begin{aligned}
&\sum_{k=i}^{n} p_k(j, t_1, t_2)\, R\big(T_{j,n}(t_1, t_2) : \nu_{k,j}\big) \\
&= \frac{1}{2} \sum_{k=i}^{n} p_k(j, t_1, t_2) \int_0^\infty \left(\bar{F}_{T_{j,n}(t_1,t_2)}(x) - \nu_{k,j}(t_1, t_2, x)\right)^2 dx \\
&= \frac{1}{2} \int_0^\infty \sum_{k=i}^{n} p_k(j, t_1, t_2) \left[\bar{F}^2_{T_{j,n}(t_1,t_2)}(x) - 2\bar{F}_{T_{j,n}(t_1,t_2)}(x)\nu_{k,j}(t_1, t_2, x) + \nu^2_{k,j}(t_1, t_2, x)\right] dx.
\end{aligned}$$

Since the weights sum to one and reproduce the mixture, the cross term simplifies, yielding

$$-\frac{1}{2} \int_0^\infty \bar{F}^2_{T_{j,n}(t_1,t_2)}(x)\, dx + \frac{1}{2} \sum_{k=i}^{n} p_k(j, t_1, t_2) \int_0^\infty \nu^2_{k,j}(t_1, t_2, x)\, dx.$$

By the definition of CRJ in (6), this equals

$$\xi J\big(T_{j,n}(t_1, t_2)\big) - \sum_{k=i}^{n} p_k(j, t_1, t_2)\, \xi J\big(\nu_{k,j}(t_1, t_2, \cdot)\big)\,,$$

which coincides with (8). □

Representation (10) shows that the inspection-conditioned divergence is nonnegative and vanishes precisely when the conditional system residual lifetime coincides with each mixture component. In particular, within the double inspection framework, the divergence measures the additional structural complexity induced by the coherent architecture, beyond that inherent in the inspection-conditioned order statistics.

Downloaded from https://www.cambridge.org/core. UNIVERSIDAD AUTONOMA METROPOLITANA, on 17 Nov 2026 at 01:28:28, subject to the Cambridge Core terms of use, available at https://www.cambridge.org/core/terms. https://doi.org/10.1017/S0269964826100369

Table 2. *Coherent systems of order* 4 *and their signature vectors.*

System	$T = \tau(X_1, X_2, X_3, X_4)$	Signature $\boldsymbol{s}$
1	$\max(X_1, X_2)$ (2-parallel)	$(0, \frac{1}{6}, \frac{1}{3}, \frac{1}{2})$
2	$\max(X_2, \min(X_1, X_3))$ (consecutive 2-out-of-3: F)	$(0, \frac{1}{3}, \frac{5}{12}, \frac{1}{4})$
3	$\max(X_1, \min(X_2, X_3, X_4))$	$(0, \frac{1}{2}, \frac{1}{4}, \frac{1}{4})$
4	$\max(X_1, \min(X_2, X_3), \min(X_3, X_4))$	$(0, \frac{1}{6}, \frac{7}{12}, \frac{1}{4})$
5	$\max(X_1, X_2, X_3)$ (3-parallel)	$(0, 0, \frac{1}{4}, \frac{3}{4})$
6	$\max(X_{2:3}, X_4)$	$(0, 0, \frac{3}{4}, \frac{1}{4})$
7	$\min(\max(X_1, X_2, X_3), \max(X_2, X_3, X_4))$	$(0, 0, \frac{1}{2}, \frac{1}{2})$
8	$\max(X_1, X_2, X_3, X_4)$ (4-parallel)	$(0, 0, 0, 1)$

3.1. Structural comparison of four-component coherent systems under Weibull components

We now specialize the inspection–conditioned framework developed in Sections 2–3 to the complete class of coherent systems of order four whose structure functions and signature vectors are summarized in Table 2. Throughout this section, component lifetimes are assumed to be IID with Weibull distribution $F(x) = 1 - \exp\left\{-\left(\frac{x}{\eta}\right)^{\beta}\right\}$, $x \geq 0$, where $\beta > 0$ and $\eta > 0$. For the numerical illustrations reported in Figures 7 and 8, we fix the Weibull parameters at $\beta = 0.8$ and $\eta = 12$. This parametric setting permits a controlled examination of how hazard shape interacts with system architecture under the double regularly checking mechanism introduced in (1)–(4).

For each system, we evaluate the conditional residual lifetime $T_{j,4}(t_1, t_2)$ under the inspection event $t_1 < X_{j:4} < t_2 < T$ and compute its CRJ via (7). Because the conditional SF admits the finite-mixture representation (1), all inspection effects enter exclusively through the signature-weighted probability vector $\boldsymbol{p}(t_1, t_2)$. Hence, any structural differentiation observed in CRJ or JCRJ is intrinsically architecture-driven.

Figure 7 displays $\xi J(T_{j,4}(t_1, t_2))$ as a function of t_1 for three fixed inspection horizons $t_2 = 0.5, 1.5, 3$. Recall that CRJ is nonpositive by definition.

The ordering below is given strictly according to the numerical values of ξJ (from largest to smallest). Because all CRJ values are negative, a larger numerical value corresponds to a value closer to zero. From the figure, the systems satisfy

$$\text{System 3} > \text{System 2} > \text{System 4} > \text{System 6} > \text{System 1} > \text{System 7} > \text{System 5} > \text{System 8},$$

where the inequality is understood in the usual numerical sense. Thus, System 3 attains the largest numerical CRJ values (least negative), whereas System 8 attains the smallest numerical CRJ values (most negative).

However, since CRJ is an inverse indicator of uncertainty, more negative values correspond to higher conditional uncertainty. Consequently, when interpreted in terms of uncertainty, the ranking is reversed: System 8 exhibits the highest inspection-conditioned uncertainty, while System 3 exhibits the lowest.

Importantly, this numerical hierarchy remains stable across $t_2 = 0.5, 1.5$, and 3. Increasing the inspection horizon t_2 shifts all curves upward toward zero, yet the relative numerical ordering across system architectures remains essentially unchanged.

We next examine the JCRJ divergence, which quantifies structural heterogeneity through the signature-weighted aggregation of relative CRJ distances (see Proposition 1). Unlike CRJ, JCRJ is nonnegative; larger values indicate greater architectural divergence between the conditional system lifetime and its order-statistic components.

Figure 8 reports JCRJ as a function of t_1 for the same inspection horizons. A complementary structural stratification is observed.

Downloaded from https://www.cambridge.org/core. UNIVERSIDAD AUTONOMA METROPOLITANA, on 17 Nov 2026 at 01:28:28, subject to the Cambridge Core terms of use, available at https://www.cambridge.org/core/terms. https://doi.org/10.1017/S0269964826100369

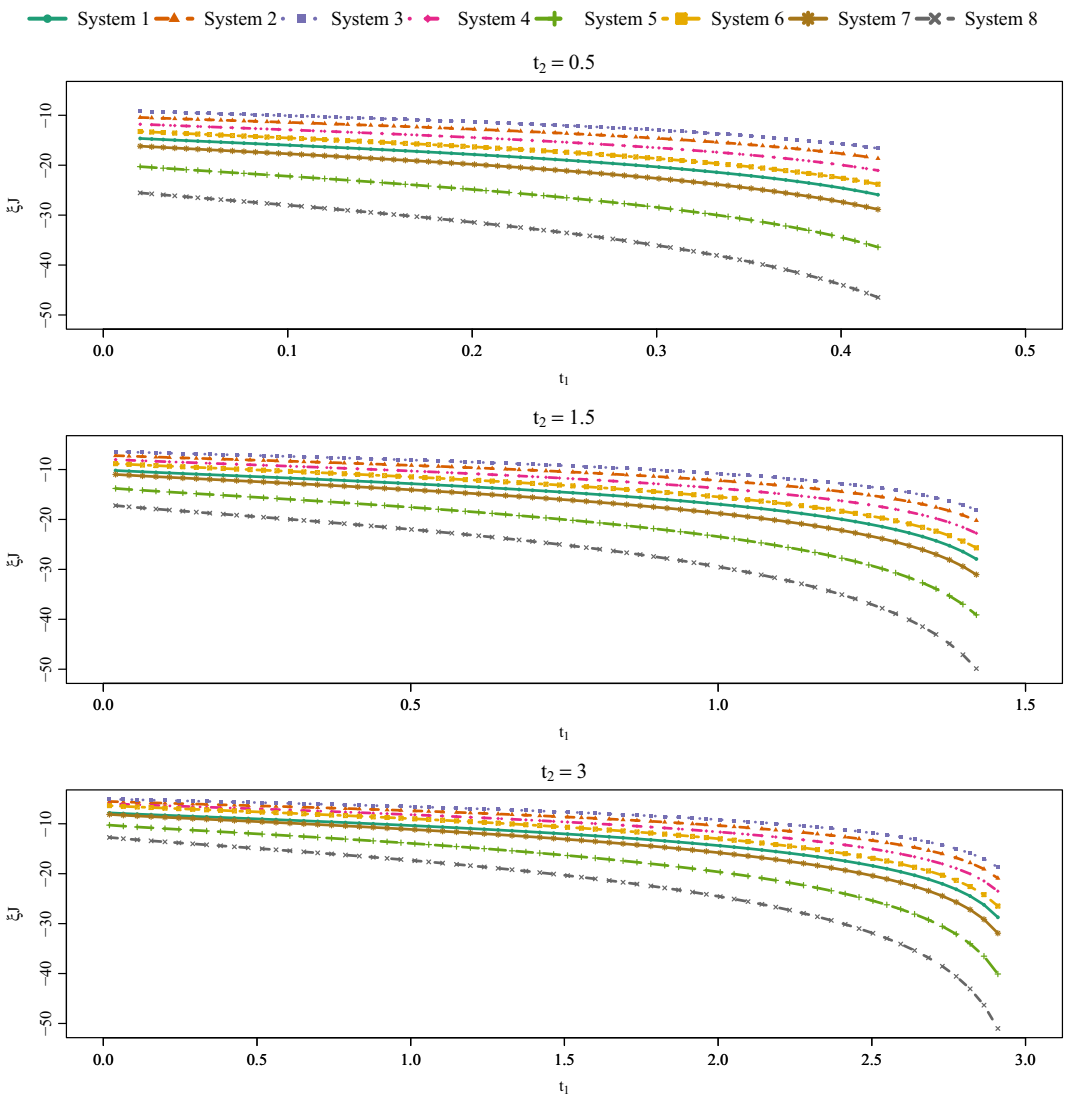


Figure 7. *CRJ values for the eight coherent systems under Weibull components, plotted versus* t_1 *for* $t_2 = 0.5, 1.5, 3$.

Hybrid and partially redundant architectures (Systems 4 and 2) consistently achieve the highest JCRJ levels, revealing substantial divergence between the system lifetime and the benchmark order statistics. Moderately redundant configurations (Systems 1, 6, and 7) form an intermediate layer. Pure parallel architectures (Systems 5 and 8) exhibit the lowest divergence, with System 8 attaining JCRJ identically equal to zero, since its lifetime coincides with the largest order statistic and no structural dispersion arises.

In contrast to CRJ, which quantifies absolute conditional uncertainty, the JCRJ index is a nonnegative divergence measure that captures structural complexity. Larger JCRJ values indicate greater architectural heterogeneity, that is, a larger deviation between the conditional system lifetime and its inspection induced order statistic benchmark. Based on the numerical results, the induced complexity ranking (from highest to lowest JCRJ) is

$$\text{System 1} \geq \text{System 3} > \text{System 2} > \text{System 7} \geq \text{System 4} > \text{System 5} = \text{System 6} > \text{System 8} = 0.$$

Downloaded from https://www.cambridge.org/core. UNIVERSIDAD AUTONOMA METROPOLITANA, on 17 Nov 2026 at 01:28:28, subject to the Cambridge Core terms of use, available at https://www.cambridge.org/core/terms. https://doi.org/10.1017/S0269964826100369

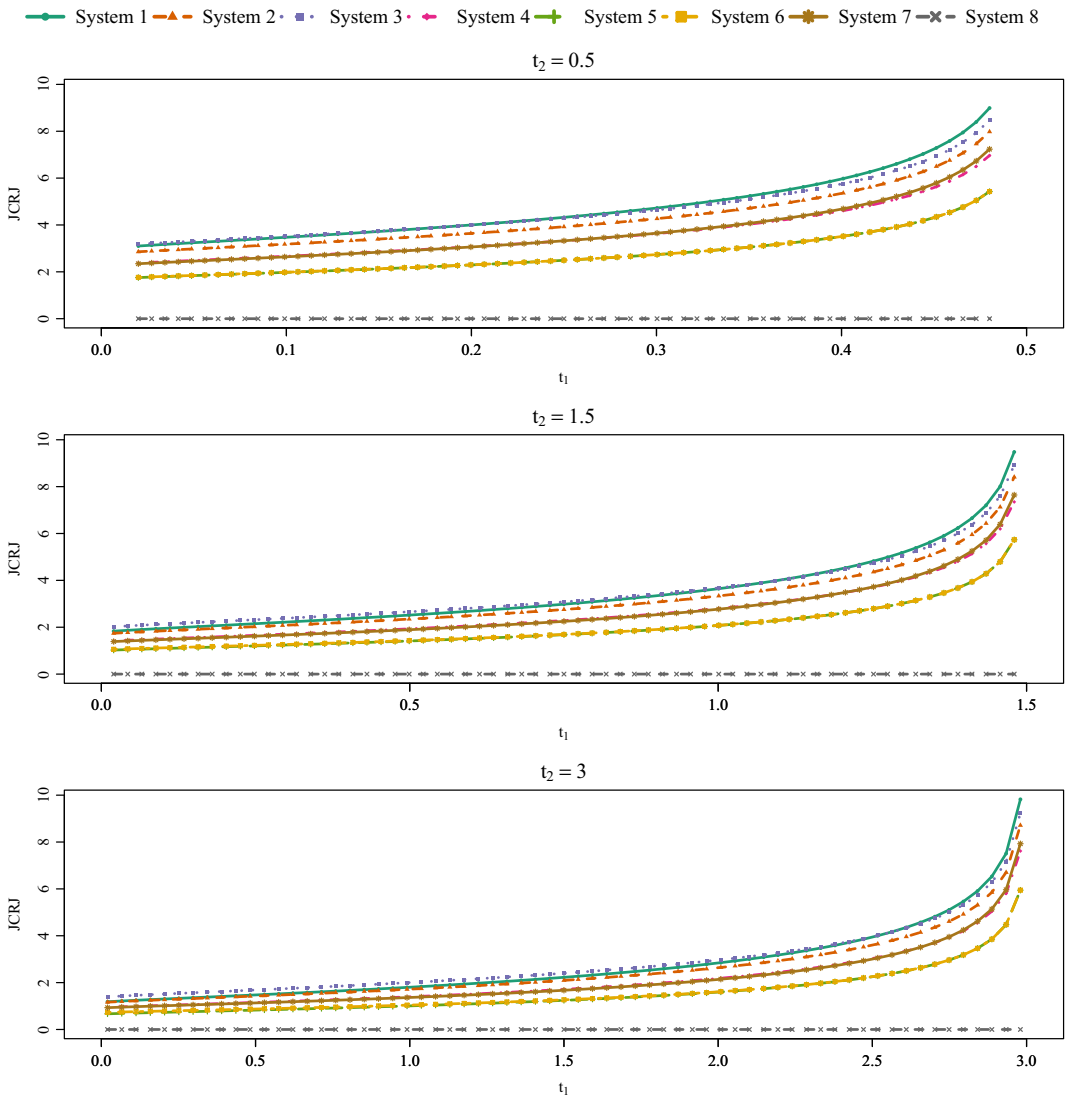


Figure 8. *JCRJ values for the eight coherent systems under Weibull components, plotted versus* t_1 *for* $t_2 = 0.5, 1.5, 3$.

Systems 1 and 3 exhibit the largest divergence values, and therefore the highest levels of structural complexity under double inspection. They are followed by Systems 2 and 7, which retain substantial architectural dispersion. Systems 5 and 6 show comparatively moderate divergence, while the fully parallel configuration (System 8) yields JCRJ identically equal to zero, reflecting the absence of structural heterogeneity: its lifetime coincides with a single order statistic, and no mixture-induced complexity arises. Increasing t_2 slightly rescales divergence magnitudes but does not alter the structural ordering. This stability indicates that JCRJ is governed primarily by the dispersion pattern of the signature vector, rather than by the inspection horizon itself.

Taken together, the CRJ–JCRJ analysis reveals two complementary informational dimensions of coherent systems under inspection:

- CRJ measures the magnitude of conditional uncertainty.
- JCRJ measures the degree of structural complexity.

Downloaded from https://www.cambridge.org/core. UNIVERSIDAD AUTONOMA METROPOLITANA, on 17 Nov 2026 at 01:28:28, subject to the Cambridge Core terms of use, available at https://www.cambridge.org/core/terms. https://doi.org/10.1017/S0269964826100369

These dimensions are fundamentally distinct. A system may exhibit low uncertainty yet high architectural complexity, or conversely, high uncertainty with limited structural dispersion. Reliability magnitude and structural complexity are therefore not synonymous notions.

Under Weibull components, the hazard shape influences the scale of both indices but does not overturn their structural hierarchy. The signature vector remains the principal determinant of inspection-conditioned informational behavior. Overall, inspection-based CRJ and JCRJ measures provide a structurally sensitive and theoretically coherent framework for discriminating coherent systems beyond classical reliability metrics.

4. Nonparametric estimation under double periodic inspections

Let $X_1, \ldots, X_N$ be an IID sample from the absolutely continuous baseline distribution function F on $[0, \infty)$. Here N denotes the sample size and should not be confused with the system size n appearing in the signature representation. Fix inspection times $0 < t_1 < t_2$ and consider the double-checking event

$$t_1 < X_{j:n} < t_2 < T(n), \qquad j = 1, \ldots, i-1.$$

Under this inspection information, the conditional SF of $T_{j,n}(t_1, t_2)$ admits the finite-mixture representation given in (1), where the mixing weights $p_k(j, t_1, t_2)$ and the conditional component SFs $\nu_{k,j}(t_1, t_2, x)$ are explicitly specified in (4) and (5), respectively. This closed-form structure permits direct plug-in and kernel-smoothed nonparametric inference for both the inspection-conditioned uncertainty index CRJ and the associated complexity index JCRJ.

4.1. Nonparametric estimators of CRJ

The CRJ of the conditional residual lifetime $T_{j,n}(t_1, t_2)$ is

$$\xi J\big(T_{j,n}(t_1, t_2)\big) = -\frac{1}{2} \int_0^\infty \left(\bar{F}_{T_{j,n}(t_1,t_2)}(x)\right)^2 dx. \tag{11}$$

Let

$$\widehat{F}_N(t) = \frac{1}{N} \sum_{r=1}^{N} \mathbf{1}\{X_r \le t\}, \qquad \widehat{\bar{F}}_N(t) = 1 - \widehat{F}_N(t).$$

Define $\widehat{p}_{k,N}$ and $\widehat{\nu}_{k,j;N}$ by substituting $\widehat{F}_N$ for F in (4) and (5). Whenever a denominator involving $\widehat{\bar{F}}_N(t_1)$ appears, use the stabilized version

$$\widehat{\bar{F}}_{N,\varepsilon}(t_1) = \max\{\widehat{\bar{F}}_N(t_1), \varepsilon_N\},$$

where $\varepsilon_N > 0$ is a deterministic sequence such that $\varepsilon_N \downarrow 0$. The resulting estimated conditional SF is

$$\widehat{\bar{F}}_{T;N}(x) = \sum_{k=i}^{n} \widehat{p}_{k,N}(j, t_1, t_2)\, \widehat{\nu}_{k,j;N}(t_1, t_2, x),$$

and the plug-in estimator of CRJ is

$$\widehat{\xi J}_N^{\text{plug}}(t_1, t_2) = -\frac{1}{2} \int_0^\infty \left(\widehat{\bar{F}}_{T;N}(x)\right)^2 dx. \tag{12}$$

Downloaded from https://www.cambridge.org/core. UNIVERSIDAD AUTONOMA METROPOLITANA, on 17 Nov 2026 at 01:28:28, subject to the Cambridge Core terms of use, available at https://www.cambridge.org/core/terms. https://doi.org/10.1017/S0269964826100369

In numerical implementation, the integral in (12) is evaluated by trapezoidal quadrature over a grid

$$0 = x_0 < \cdots < x_M = x_{\max},$$

where $x_{\max}$ is chosen sufficiently large so that the tail contribution is negligible.

To reduce the staircase effect induced by the empirical distribution function at the points t_1, t_2, and $t_2 + x$, consider the smoothed estimator

$$\widehat{F}_{N,h}(t) = \frac{1}{N}\sum_{r=1}^{N} \Phi\left(\frac{t - X_r}{h}\right), \qquad \widehat{\bar{F}}_{N,h}(t) = 1 - \widehat{F}_{N,h}(t),$$

where Φ denotes the standard normal distribution function and $h = h_N \downarrow 0$. Define $\widehat{p}_{k,N,h}$ and $\widehat{\nu}_{k,j;N,h}$ by substituting $\widehat{F}_{N,h}$ into (4) and (5), and set

$$\widehat{\bar{F}}_{T;N,h}(x) = \sum_{k=i}^{n} \widehat{p}_{k,N,h}(j, t_1, t_2)\, \widehat{\nu}_{k,j;N,h}(t_1, t_2, x).$$

Then the kernel-smoothed CRJ estimator is

$$\widehat{\xi J}_N^{\ker}(t_1, t_2) = -\frac{1}{2}\int_0^{\infty} \left(\widehat{\bar{F}}_{T;N,h}(x)\right)^2 dx. \tag{13}$$

Assumption 1. *Fix $0 < t_1 < t_2$ such that $0 < F(t_1) < F(t_2) < 1$, and assume*

$$\int_0^{\infty} \left(\bar{F}_{T_{j,n}(t_1,t_2)}(x)\right)^2 dx < \infty.$$

For the stabilized plug-in estimator, assume also that $\varepsilon_N \downarrow 0$ almost surely. For the kernel estimator, assume $h_N \downarrow 0$ and $Nh_N \longrightarrow \infty$ as $N \longrightarrow \infty$.

Lemma 1. *Under Assumption 1, for each fixed $x \geq 0$, the mapping*

$$F \mapsto \bar{F}_{T_{j,n}(t_1,t_2)}(x)$$

is continuous with respect to pointwise convergence of $F(t_1)$, $F(t_2)$, and $F(t_2 + x)$. Moreover,

$$0 \leq \bar{F}_{T_{j,n}(t_1,t_2)}(x) \leq 1, \qquad x \geq 0.$$

Proof. Fix $x \geq 0$. By (4), the mixing weights $p_k(j, t_1, t_2)$ are ratios of finite sums of products involving the scalars $F(t_1)$, $F(t_2) - F(t_1)$, and $1 - F(t_2)$, multiplied by binomial coefficients and signature weights. On the interior region $0 < F(t_1) < F(t_2) < 1$, the normalizing denominator in (4) is strictly positive. Hence each $p_k(j, t_1, t_2)$ is a continuous function of $(F(t_1), F(t_2))$, and the vector $(p_i, \ldots, p_n)$ forms a probability vector.

Next, by (5), the component term $\nu_{k,j}(t_1, t_2, x)$ is also expressed as a ratio of finite sums depending on F only through

$$\phi(t_1) = \frac{F(t_1)}{1 - F(t_1)} \qquad \text{and} \qquad F(x \mid t_1, t_2) = \frac{F(t_2 + x) - F(t_1)}{1 - F(t_1)}.$$

Under $0 < F(t_1) < F(t_2) < 1$, these quantities are well-defined and vary continuously with $F(t_1)$, $F(t_2)$, and $F(t_2 + x)$. The denominator in (5) is again strictly positive, and therefore $\nu_{k,j}(t_1, t_2, x)$ is continuous

Downloaded from https://www.cambridge.org/core. UNIVERSIDAD AUTONOMA METROPOLITANA, on 17 Nov 2026 at 01:28:28, subject to the Cambridge Core terms of use, available at https://www.cambridge.org/core/terms. https://doi.org/10.1017/S0269964826100369

in the same arguments. Since it is a conditional SF, it satisfies

$$0 \le \nu_{k,j}(t_1, t_2, x) \le 1.$$

Finally, using the mixture representation (1),

$$\bar{F}_{T_{j,n}(t_1,t_2)}(x) = \sum_{k=i}^{n} p_k(j, t_1, t_2)\, \nu_{k,j}(t_1, t_2, x),$$

which is a finite convex combination of terms in $[0, 1]$ with weights summing to one. Hence

$$0 \le \bar{F}_{T_{j,n}(t_1,t_2)}(x) \le 1,$$

and the asserted continuity follows. □

Theorem 3 *Under Assumption 1,*

$$\widehat{\xi J}_N^{\text{plug}}(t_1, t_2) \xrightarrow{\text{a.s.}} \xi J\big(T_{j,n}(t_1, t_2)\big), \qquad N \to \infty.$$

Proof. By the Glivenko–Cantelli theorem,

$$\sup_{t \ge 0} |\widehat{F}_N(t) - F(t)| \to 0 \qquad \text{a.s.}$$

Hence, for each fixed $x \ge 0$,

$$\widehat{F}_N(t_1) \to F(t_1), \qquad \widehat{F}_N(t_2) \to F(t_2), \qquad \widehat{F}_N(t_2 + x) \to F(t_2 + x)$$

almost surely. Because $\varepsilon_N \downarrow 0$, the stabilization does not alter the limit. Lemma 1 therefore yields

$$\widehat{\bar{F}}_{T;N}(x) \to \bar{F}_{T_{j,n}(t_1,t_2)}(x) \qquad \text{a.s. for each fixed } x \ge 0.$$

Moreover,

$$0 \le \widehat{\bar{F}}_{T;N}(x) \le 1, \qquad 0 \le \bar{F}_{T_{j,n}(t_1,t_2)}(x) \le 1.$$

Under Assumption 1, the integrand is square-integrable in the limit, and the same boundedness provides domination on every finite interval. Consequently,

$$\int_0^\infty \left(\widehat{\bar{F}}_{T;N}(x)\right)^2 dx \to \int_0^\infty \left(\bar{F}_{T_{j,n}(t_1,t_2)}(x)\right)^2 dx \qquad \text{a.s.}$$

and multiplying by $-1/2$ proves the result. □

Downloaded from https://www.cambridge.org/core. UNIVERSIDAD AUTONOMA METROPOLITANA, on 17 Nov 2026 at 01:28:28, subject to the Cambridge Core terms of use, available at https://www.cambridge.org/core/terms. https://doi.org/10.1017/S0269964826100369

Theorem 4 *Under Assumption 1,*

$$\widehat{\xi J}_N^{\ker}(t_1,t_2) \xrightarrow{p} \xi J\big(T_{j,n}(t_1,t_2)\big), \qquad N \to \infty.$$

Proof. For each fixed $t \geq 0$, standard kernel distribution theory implies

$$\widehat{F}_{N,h}(t) \to F(t) \qquad \text{in probability}$$

whenever $h_N \downarrow 0$ and $Nh_N \to \infty$. Therefore, for each fixed $x \geq 0$,

$$\big(\widehat{F}_{N,h}(t_1), \widehat{F}_{N,h}(t_2), \widehat{F}_{N,h}(t_2+x)\big) \to \big(F(t_1), F(t_2), F(t_2+x)\big)$$

in probability. By Lemma 1,

$$\widehat{\bar{F}}_{T;N,h}(x) \to \bar{F}_{T_{j,n}(t_1,t_2)}(x) \qquad \text{in probability for each fixed } x \geq 0.$$

Again,

$$0 \leq \widehat{\bar{F}}_{T;N,h}(x) \leq 1.$$

Combining this boundedness with Assumption 1 yields convergence in probability of the quadratic integral, and the claim follows. □

Proposition 2. *For any N and any $h > 0$, the numerically truncated estimators computed on $[0, x_{\max}]$ satisfy*

$$-\frac{1}{2}x_{\max} \leq \widehat{\xi J}_N^{*}(t_1,t_2) \leq 0, \qquad * \in \{\text{plug}, \ker\},$$

whenever the estimated conditional SF is well-defined.

Proof. Since

$$0 \leq \widehat{\bar{F}}_{T;\cdot}(x) \leq 1,$$

we have

$$0 \leq \big(\widehat{\bar{F}}_{T;\cdot}(x)\big)^2 \leq 1 \qquad \text{for } x \in [0, x_{\max}].$$

Therefore,

$$0 \leq \int_0^{x_{\max}} \big(\widehat{\bar{F}}_{T;\cdot}(x)\big)^2 \, dx \leq x_{\max}.$$

Multiplying by $-1/2$ gives the stated bound. □

Downloaded from https://www.cambridge.org/core. UNIVERSIDAD AUTONOMA METROPOLITANA, on 17 Nov 2026 at 01:28:28, subject to the Cambridge Core terms of use, available at https://www.cambridge.org/core/terms. https://doi.org/10.1017/S0269964826100369

4.2. Nonparametric estimators of JCRJ

The inspection-conditioned JCRJ divergence is defined by

$$\mathrm{JCRJ}_{j,n}(t_1,t_2) = \xi J\big(T_{j,n}(t_1,t_2)\big) - \sum_{k=i}^{n} p_k(j,t_1,t_2)\,\xi J\big(\nu_{k,j}(t_1,t_2,\cdot)\big)\,, \tag{14}$$

where

$$\xi J\big(\nu_{k,j}(t_1,t_2,\cdot)\big) = -\frac{1}{2}\int_0^\infty \Big(\nu_{k,j}(t_1,t_2,x)\Big)^2\,dx.$$

Using the plug-in quantities introduced above, define

$$\widehat{\xi J}_N^{\,\mathrm{plug}}\big(\nu_{k,j}\big) = -\frac{1}{2}\int_0^\infty \big(\widehat{\nu}_{k,j;N}(t_1,t_2,x)\big)^2\,dx, \qquad k=i,\dots,n,$$

and set

$$\widehat{\mathrm{JCRJ}}_N^{\,\mathrm{plug}}(t_1,t_2) = \widehat{\xi J}_N^{\,\mathrm{plug}}(t_1,t_2) - \sum_{k=i}^{n} \widehat{p}_{k,N}(j,t_1,t_2)\,\widehat{\xi J}_N^{\,\mathrm{plug}}\big(\nu_{k,j}\big)\,. \tag{15}$$

Analogously, using $\widehat{p}_{k,N,h}$ and $\widehat{\nu}_{k,j;N,h}$, define

$$\widehat{\xi J}_N^{\,\mathrm{ker}}\big(\nu_{k,j}\big) = -\frac{1}{2}\int_0^\infty \big(\widehat{\nu}_{k,j;N,h}(t_1,t_2,x)\big)^2\,dx, \qquad k=i,\dots,n,$$

and

$$\widehat{\mathrm{JCRJ}}_N^{\,\mathrm{ker}}(t_1,t_2) = \widehat{\xi J}_N^{\,\mathrm{ker}}(t_1,t_2) - \sum_{k=i}^{n} \widehat{p}_{k,N,h}(j,t_1,t_2)\,\widehat{\xi J}_N^{\,\mathrm{ker}}\big(\nu_{k,j}\big)\,. \tag{16}$$

Assumption 2. *Assume Assumption 1. In addition, for each* $k=i,\dots,n$,

$$\int_0^\infty \Big(\nu_{k,j}(t_1,t_2,x)\Big)^2\,dx < \infty.$$

Proposition 3. *For fixed* (t_1,t_2),

$$\mathrm{JCRJ}_{j,n}(t_1,t_2) \geq 0.$$

Moreover, whenever the estimated quantities are well-defined,

$$\widehat{\mathrm{JCRJ}}_N^{\,\mathrm{plug}}(t_1,t_2) \geq 0, \qquad \widehat{\mathrm{JCRJ}}_N^{\,\mathrm{ker}}(t_1,t_2) \geq 0.$$

Proof. Suppress (j,t_1,t_2) for brevity and write

$$\bar{S}(x) = \bar{F}_T(x) = \sum_{k=i}^{n} p_k \nu_k(x), \qquad \sum_{k=i}^{n} p_k = 1.$$

Downloaded from https://www.cambridge.org/core. UNIVERSIDAD AUTONOMA METROPOLITANA, on 17 Nov 2026 at 01:28:28, subject to the Cambridge Core terms of use, available at https://www.cambridge.org/core/terms. https://doi.org/10.1017/S0269964826100369

Then

$$\mathrm{JCRJ} = -\frac{1}{2}\int_0^\infty \bar{S}(x)^2\,dx + \frac{1}{2}\sum_{k=i}^{n} p_k \int_0^\infty \nu_k(x)^2\,dx.$$

Using the identity

$$\sum_{k=i}^{n} p_k\big(\bar{S}(x) - \nu_k(x)\big)^2 = \sum_{k=i}^{n} p_k \nu_k(x)^2 - \bar{S}(x)^2,$$

which follows from $\bar{S}(x) = \sum_{k=i}^{n} p_k \nu_k(x)$ and $\sum_{k=i}^{n} p_k = 1$, we obtain

$$\mathrm{JCRJ} = \frac{1}{2}\sum_{k=i}^{n} p_k \int_0^\infty \big(\bar{S}(x) - \nu_k(x)\big)^2\,dx \geq 0.$$

The same argument applies to the plug-in and kernel estimators after replacing $(p_k, \nu_k, \bar{S})$ by their estimated counterparts. Since the estimated conditional SF remains a convex combination of the estimated component SFs, both estimators are nonnegative whenever they are well-defined. □

Theorem 5 *Under Assumption 2,*

$$\widehat{\mathrm{JCRJ}}_N^{\mathrm{plug}}(t_1, t_2) \xrightarrow{\text{a.s.}} \mathrm{JCRJ}_{j,n}(t_1, t_2), \qquad N \to \infty.$$

Proof. By Theorem 3,

$$\widehat{\xi J}_N^{\mathrm{plug}}(t_1, t_2) \to \xi J\big(T_{j,n}(t_1, t_2)\big) \qquad \text{a.s.}$$

For each fixed $k = i, \ldots, n$, pointwise almost sure convergence

$$\widehat{\nu}_{k,j;N}(t_1, t_2, x) \to \nu_{k,j}(t_1, t_2, x)$$

follows from the same continuity argument used above together with (5). Since

$$0 \leq \widehat{\nu}_{k,j;N}(t_1, t_2, x) \leq 1, \qquad 0 \leq \nu_{k,j}(t_1, t_2, x) \leq 1,$$

Assumption 2 implies

$$\widehat{\xi J}_N^{\mathrm{plug}}\big(\nu_{k,j}\big) \to \xi J\big(\nu_{k,j}(t_1, t_2, \cdot)\big) \qquad \text{a.s.}$$

Also,

$$\widehat{p}_{k,N}(j, t_1, t_2) \to p_k(j, t_1, t_2) \qquad \text{a.s.}$$

by continuity of (4). Since (15) is a finite sum of strongly consistent terms, the claim follows. □

Downloaded from https://www.cambridge.org/core. UNIVERSIDAD AUTONOMA METROPOLITANA, on 17 Nov 2026 at 01:28:28, subject to the Cambridge Core terms of use, available at https://www.cambridge.org/core/terms. https://doi.org/10.1017/S0269964826100369

Theorem 6 *Under Assumption 2,*

$$\widehat{\mathrm{JCRJ}}_N^{\ker}(t_1,t_2) \xrightarrow{p} \mathrm{JCRJ}_{j,n}(t_1,t_2), \qquad N \to \infty.$$

Proof. Under Assumption 1, for each fixed t, the smoothed estimator satisfies

$$\widehat{F}_{N,h}(t) \to F(t) \qquad \text{in probability.}$$

Therefore, for each fixed $k = i, \ldots, n$ and $x \geq 0$,

$$\widehat{p}_{k,N,h}(j,t_1,t_2) \to p_k(j,t_1,t_2) \qquad \text{and} \qquad \widehat{\nu}_{k,j;N,h}(t_1,t_2,x) \to \nu_{k,j}(t_1,t_2,x)$$

in probability, by continuity of (4) and (5). Using again the boundedness of the estimated component SFs together with Assumption 2, we obtain

$$\widehat{\xi J}_N^{\ker}\left(\nu_{k,j}\right) \to \xi J\left(\nu_{k,j}(t_1,t_2,\cdot)\right) \qquad \text{in probability,}$$

as well as

$$\widehat{\xi J}_N^{\ker}(t_1,t_2) \to \xi J\left(T_{j,n}(t_1,t_2)\right) \qquad \text{in probability.}$$

Substituting these convergences into (16) and applying Slutsky's theorem completes the proof. □

Remark 1. The estimators are computationally convenient because (4) and (5) depend on the baseline distribution function only through evaluations at t_1, t_2, and $t_2 + x$. Consequently, both empirical substitution and kernel smoothing are immediate to implement. Moreover, all survival quantities involved lie in $[0, 1]$, which is helpful for stable numerical integration.

4.3. Asymptotic normality, influence functions, and variance estimation

The preceding results establish consistency. We now derive the first-order limiting distribution of the plug-in estimators, together with their influence functions and consistent variance estimators. Throughout, fix (j, n, i, t_1, t_2) and write

$$a = F(t_1), \qquad b = F(t_2), \qquad c_x = F(t_2 + x).$$

Because the mixing weights depend on F only through (a, b) and the conditional components depend on F only through (a, c_x), the conditional SF in (1) may be written as

$$\bar{S}_F(x) = \mathcal{S}(a,b,c_x) = \sum_{k=i}^{n} p_k(a,b)\, \nu_{k,j}(a,c_x).$$

Define

$$g_1(x) = \partial_a \mathcal{S}(a,b,c_x), \qquad g_2(x) = \partial_b \mathcal{S}(a,b,c_x), \qquad g_3(x) = \partial_c \mathcal{S}(a,b,c)\big|_{c=c_x}.$$

Equivalently,

$$g_1(x) = \sum_{k=i}^{n} \left[\partial_a p_k(a,b)\, \nu_{k,j}(a,c_x) + p_k(a,b)\, \partial_a \nu_{k,j}(a,c_x)\right],$$

Downloaded from https://www.cambridge.org/core. UNIVERSIDAD AUTONOMA METROPOLITANA, on 17 Nov 2026 at 01:28:28, subject to the Cambridge Core terms of use, available at https://www.cambridge.org/core/terms. https://doi.org/10.1017/S0269964826100369

$$g_2(x) = \sum_{k=i}^{n} \partial_b p_k(a,b)\, \nu_{k,j}(a,c_x), \qquad g_3(x) = \sum_{k=i}^{n} p_k(a,b)\, \partial_c \nu_{k,j}(a,c)\big|_{c=c_x}.$$

Assumption 3. *In addition to Assumption 2, assume that F is absolutely continuous, $0 < F(t_1) < F(t_2) < 1$, and*

$$\int_0^\infty |\bar{S}_F(x)|\Big(|g_1(x)| + |g_2(x)| + |g_3(x)|\Big)\, dx < \infty,$$

together with

$$\int_0^\infty \bar{S}_F(x)^2\, dx < \infty.$$

Assume also the analogous integrability conditions for each component functional

$$\xi J\big(\nu_{k,j}(t_1,t_2,\cdot)\big)$$

and its first-order derivatives with respect to the relevant arguments, so that all influence functions appearing below are square integrable.

Theorem 7 (Asymptotic normality of the plug-in CRJ) *Under Assumption 3,*

$$\sqrt{N}\Big(\widehat{\xi J}_N^{\,\mathrm{plug}}(t_1,t_2) - \xi J\big(T_{j,n}(t_1,t_2)\big)\Big) \xrightarrow{d} \mathcal{N}\big(0, \sigma^2_{\mathrm{CRJ}}\big),$$

where

$$\sigma^2_{\mathrm{CRJ}} = \mathbb{E}\big[\psi_{\mathrm{CRJ}}(X_1)^2\big],$$

and the influence function is

$$\psi_{\mathrm{CRJ}}(z) = A_1\big(\mathbf{1}\{z \le t_1\} - F(t_1)\big) + A_2\big(\mathbf{1}\{z \le t_2\} - F(t_2)\big) - \Big(H\big((z-t_2)_+\big) - c_3\Big),$$

with

$$A_1 = -\int_0^\infty \bar{S}_F(x)\, g_1(x)\, dx, \qquad A_2 = -\int_0^\infty \bar{S}_F(x)\, g_2(x)\, dx,$$

$$H(u) = \int_u^\infty \bar{S}_F(x)\, g_3(x)\, dx, \qquad c_3 = \int_0^\infty \bar{S}_F(x)\, g_3(x)\, F(t_2+x)\, dx.$$

Proof. Define the functional

$$\theta(G) = -\frac{1}{2}\int_0^\infty \bar{S}_G(x)^2\, dx,$$

where

$$\bar{S}_G(x) = \mathcal{S}\big(G(t_1), G(t_2), G(t_2+x)\big).$$

Under Assumption 3, the map $G \mapsto \bar{S}_G(x)$ is differentiable at F, and differentiation under the integral sign is justified by the stated integrability conditions. Hence the Hadamard derivative of θ at F in the

Downloaded from https://www.cambridge.org/core. UNIVERSIDAD AUTONOMA METROPOLITANA, on 17 Nov 2026 at 01:28:28, subject to the Cambridge Core terms of use, available at https://www.cambridge.org/core/terms. https://doi.org/10.1017/S0269964826100369

direction η is

$$D\theta_F[\eta] = -\int_0^\infty \bar{S}_F(x)\Big[g_1(x)\eta(t_1) + g_2(x)\eta(t_2) + g_3(x)\eta(t_2+x)\Big]\,dx.$$

Since

$$\sqrt{N}(\widehat{F}_N - F)$$

converges weakly to an F-Brownian bridge, the functional delta method implies

$$\sqrt{N}\big(\theta(\widehat{F}_N) - \theta(F)\big) \xrightarrow{d} \mathcal{N}(0, \sigma^2_{\mathrm{CRJ}}),$$

with influence function

$$\psi_{\mathrm{CRJ}}(z) = D\theta_F[\delta_z - F].$$

Substituting $\eta = \delta_z - F$ gives

$$\psi_{\mathrm{CRJ}}(z) = -\int_0^\infty \bar{S}_F(x)\Big[g_1(x)\big(\mathbf{1}\{z \le t_1\} - F(t_1)\big) + g_2(x)\big(\mathbf{1}\{z \le t_2\} - F(t_2)\big) + g_3(x)\big(\mathbf{1}\{z \le t_2 + x\} - F(t_2+x)\big)\Big]\,dx.$$

Now

$$\mathbf{1}\{z \le t_2 + x\} = \mathbf{1}\{x \ge (z - t_2)_+\},$$

and therefore Fubini's theorem yields

$$\int_0^\infty \bar{S}_F(x)\, g_3(x)\, \mathbf{1}\{z \le t_2 + x\}\,dx = \int_{(z-t_2)_+}^\infty \bar{S}_F(x)\, g_3(x)\,dx = H\big((z-t_2)_+\big),$$

which gives the stated form. The variance representation follows from $\mathbb{E}[\psi_{\mathrm{CRJ}}(X_1)] = 0$. □

Theorem 8 (Asymptotic normality of the plug-in JCRJ) *Under Assumption 3,*

$$\sqrt{N}\Big(\widehat{\mathrm{JCRJ}}_N^{\,\mathrm{plug}}(t_1,t_2) - \mathrm{JCRJ}_{j,n}(t_1,t_2)\Big) \xrightarrow{d} \mathcal{N}\big(0, \sigma^2_{\mathrm{JCRJ}}\big),$$

where

$$\sigma^2_{\mathrm{JCRJ}} = \mathbb{E}\big[\psi_{\mathrm{JCRJ}}(X_1)^2\big],$$

and

$$\psi_{\mathrm{JCRJ}}(z) = \psi_{\mathrm{CRJ}}(z) - \sum_{k=i}^{n}\big[\dot{p}_k(z)\,\theta_k(F) + p_k(F)\,\psi_{\theta_k}(z)\big],$$

with

$$\theta_k(F) = \xi J\big(\nu_{k,j}(t_1,t_2,\cdot)\big),$$

Downloaded from https://www.cambridge.org/core. UNIVERSIDAD AUTONOMA METROPOLITANA, on 17 Nov 2026 at 01:28:28, subject to the Cambridge Core terms of use, available at https://www.cambridge.org/core/terms. https://doi.org/10.1017/S0269964826100369

$$\dot{p}_k(z) = \partial_a p_k(a,b)\big(\mathbf{1}\{z \le t_1\} - F(t_1)\big) + \partial_b p_k(a,b)\big(\mathbf{1}\{z \le t_2\} - F(t_2)\big),$$

and

$$\psi_{\theta_k}(z) = -\int_0^\infty \nu_{k,j}(t_1,t_2,x)\Big[\partial_a \nu_{k,j}(a,c_x)\big(\mathbf{1}\{z \le t_1\} - F(t_1)\big) + \partial_c \nu_{k,j}(a,c)\big|_{c=c_x}\big(\mathbf{1}\{z \le t_2 + x\} - F(t_2+x)\big)\Big]\,dx.$$

Proof. Consider the functional

$$\Theta(F) = \xi J\big(T_{j,n}(t_1,t_2)\big) - \sum_{k=i}^{n} p_k(F)\,\theta_k(F).$$

The first term has influence function $\psi_{\mathrm{CRJ}}(z)$ by Theorem 7. For each k, the weight $p_k(F)$ depends only on $(F(t_1), F(t_2))$, hence its influence function is $\dot{p}_k(z)$. Likewise, $\theta_k(F)$ is a quadratic functional of the same general form as the CRJ functional, and its influence function is $\psi_{\theta_k}(z)$. Applying the product rule for Hadamard derivatives to $p_k(F)\theta_k(F)$ and summing over k gives

$$\psi_{\mathrm{JCRJ}}(z) = \psi_{\mathrm{CRJ}}(z) - \sum_{k=i}^{n}\left[\dot{p}_k(z)\,\theta_k(F) + p_k(F)\,\psi_{\theta_k}(z)\right].$$

The conclusion then follows from the functional delta method. □

A consistent variance estimator is obtained by empirical influence-function substitution. Replace F by $\widehat{F}_N$ throughout ψ_{CRJ} and ψ_{JCRJ}, using the same stabilization as in the point estimators whenever necessary, and evaluate the resulting integrals numerically. If the estimated influence values are denoted by $\widehat{\psi}_\bullet(X_r)$, then

$$\widehat{\sigma}^2_\bullet = \frac{1}{N}\sum_{r=1}^{N} \widehat{\psi}_\bullet(X_r)^2, \qquad \bullet \in \{\mathrm{CRJ}, \mathrm{JCRJ}\}, \tag{17}$$

is consistent for $\sigma^2_\bullet$. Therefore, the asymptotic standard error is

$$\widehat{\mathrm{SE}}_\bullet = \frac{\widehat{\sigma}_\bullet}{\sqrt{N}},$$

and an approximate two-sided $(1-\alpha)$ confidence interval is

$$\widehat{\theta}_\bullet \pm z_{1-\alpha/2}\,\widehat{\mathrm{SE}}_\bullet.$$

Corollary 1. (Kernel estimators) *Assume, in addition, that*

$$\sqrt{N}\,h_N^2 \to 0.$$

Then the kernel-smoothed estimators $\widehat{\xi J}_N^{\,\mathrm{ker}}(t_1,t_2)$ *and* $\widehat{\mathrm{JCRJ}}_N^{\,\mathrm{ker}}(t_1,t_2)$ *have the same asymptotic distributions as their plug-in counterparts, with the same asymptotic variances.*

Downloaded from https://www.cambridge.org/core. UNIVERSIDAD AUTONOMA METROPOLITANA, on 17 Nov 2026 at 01:28:28, subject to the Cambridge Core terms of use, available at https://www.cambridge.org/core/terms. https://doi.org/10.1017/S0269964826100369

Proof. Under the stated bandwidth condition, the smoothing bias is of smaller order than $N^{-1/2}$, whereas the stochastic part is asymptotically equivalent to that of the empirical distribution function. Hence the kernel-smoothed estimators are asymptotically equivalent to the corresponding plug-in estimators, and the result follows from Slutsky's theorem. □

The plug-in and kernel-smoothed estimators developed in this section assume that complete lifetime observations of the system components are available. In practice, when only interval-censored data between inspections are recorded, one would need to employ appropriate methods for estimating the underlying CDF F before applying the CRJ/JCRJ formulas.

4.4. Monte Carlo assessment for CRJ and JCRJ estimators

We assess the finite-sample performance of the proposed nonparametric estimators of $\xi J\big(T_{j,n}(t_1,t_2)\big)$ and $\mathrm{JCRJ}_{j,n}(t_1,t_2)$ under the double periodic inspection model. In each Monte Carlo replicate, an IID sample $X_1,\ldots,X_N$ is generated from a baseline component distribution F on $[0,\infty)$. The plug-in estimators are obtained by substituting the empirical CDF $\widehat{F}_N$ into the closed-form expressions (4) and (5), and then evaluating the defining quadratic integrals in (12) and (15) by trapezoidal quadrature. To reduce staircase variability at the inspection points t_1, t_2 and at t_2+x, a kernel-smoothed version is constructed by replacing $\widehat{F}_N$ with $\widehat{F}_{N,h}(t) = N^{-1}\sum_{r=1}^{N}\Phi((t-X_r)/h)$, leading to (13) and (16).

We report the Monte Carlo bias and RMSE for sample sizes $N \in \{20, 30, 50, 100\}$ and system sizes $n \in \{5, 7, 10, 15\}$. The inspection times are fixed at $(t_1, t_2) = (1, 2)$. To ensure that both uncertainty (CRJ) and structural complexity (JCRJ) are nondegenerate, we adopt the signature vector

$$\boldsymbol{s} = (0,\ldots,0,\tfrac{1}{2},\tfrac{1}{2}), \qquad i = n-1, \qquad \text{and set} \qquad j = n-2.$$

Each configuration is replicated $B = 5,000$ times. The kernel bandwidth is chosen by the heuristic rule $h = \lfloor\sqrt{N} + 0.5\rfloor \cdot \widehat{\sigma}\, N^{-1/5}$, where $\widehat{\sigma}$ is the sample standard deviation.

Recall that $\xi J\big(T_{j,n}(t_1,t_2)\big)$ is an absolute uncertainty index for the inspection-conditioned residual lifetime: since CRJ is nonpositive by definition, values closer to zero correspond to lower uncertainty, while more negative values indicate higher uncertainty. In contrast, $\mathrm{JCRJ}_{j,n}(t_1,t_2)$ is a nonnegative divergence and is interpreted as a structural complexity index: larger values indicate greater discrepancy between the conditional system residual lifetime and its inspection-induced benchmark components, hence greater complexity.

We first consider lognormal component lifetimes with parameters $(\mu,\sigma) = (0.5, 0.8)$. Table 3 summarizes the Monte Carlo bias and RMSE for both estimators. For CRJ, the kernel estimator is uniformly competitive and typically yields a smaller RMSE than the plug-in estimator, especially for smaller samples (e.g., $N = 20, 30$ across all n), reflecting the benefit of smoothing the staircase behavior of $\widehat{F}_N$ at the inspection points. As N increases, RMSE decreases for both estimators, consistent with convergence of the estimated CDF increments entering (4) and (5). For JCRJ, both estimators remain numerically stable across the full grid of (n, N) and exhibit small bias and RMSE at moderate and large sample sizes, indicating that the proposed complexity estimator is well-behaved even under a relatively heavy-tailed baseline. Overall, Table 3 indicates that smoothing is particularly beneficial for CRJ in small samples, whereas JCRJ is robustly estimable throughout.

We next consider Weibull components with parameters $(\text{shape}, \text{scale}) = (1.3, 1.5)$. Table 4 shows that CRJ estimation is substantially more accurate than in the lognormal case: RMSE levels are smaller across most (n, N), consistent with the smoother and lighter-tailed nature of the Weibull model at the inspection arguments. Kernel smoothing continues to improve the CRJ RMSE at small N (notably $N = 20, 30$), while the gap narrows as N grows, as expected from asymptotic consistency. For JCRJ, both estimators produce small RMSE values across all configurations, indicating that the architecture-sensitive complexity index is estimated reliably. The stability of the JCRJ columns, together with

Downloaded from https://www.cambridge.org/core. UNIVERSIDAD AUTONOMA METROPOLITANA, on 17 Nov 2026 at 01:28:28, subject to the Cambridge Core terms of use, available at https://www.cambridge.org/core/terms. https://doi.org/10.1017/S0269964826100369

Table 3. *Monte Carlo comparison of nonparametric estimators of* $\xi J\left(T_{j,n}(t_1,t_2)\right)$ *and* $\mathrm{JCRJ}_{j,n}(t_1,t_2)$ *under Lognormal* $(\mu=0,\sigma=0.8)$ *components (double inspection at* $t_1=1$, $t_2=2$*).*

		CRJ				JCRJ			
		Plug-in		Kernel		Plug-in		Kernel	
n_{sys}	N_{sample}	Bias	RMSE	Bias	RMSE	Bias	RMSE	Bias	RMSE
5	20	−0.38035	2.18442	−0.10655	0.34626	0.03761	0.43781	0.00764	0.04036
5	30	−0.17658	1.25571	−0.07406	0.27200	0.00757	0.04323	0.00673	0.03222
5	50	−0.06152	0.21273	−0.03243	0.18035	0.00373	0.02670	0.00341	0.02073
5	100	−0.03533	0.13850	−0.02221	0.12227	0.00222	0.01290	0.00281	0.01223
7	20	−0.52842	3.00372	−0.14632	0.45777	0.00661	0.04997	0.00764	0.04362
7	30	−0.24323	1.75126	−0.10367	0.36692	0.00901	0.04979	0.00931	0.04714
7	50	−0.05946	0.25166	−0.05077	0.24177	0.00324	0.02592	0.00444	0.02399
7	100	−0.04567	0.17845	−0.04803	0.17609	0.00396	0.02019	0.00589	0.01975
10	20	−0.68301	3.55710	−0.21974	0.99201	−0.00044	0.11356	0.00760	0.13321
10	30	−0.17006	0.60380	−0.18384	0.60581	0.00977	0.07679	0.01397	0.07839
10	50	−0.08229	0.38747	−0.10980	0.39857	0.00443	0.04664	0.00884	0.04640
10	100	−0.07295	0.28794	−0.11290	0.30619	0.00648	0.03614	0.01222	0.03744
15	20	−0.44279	3.29392	−0.12548	1.13841	−0.08921	0.12459	−0.06897	0.12816
15	30	−0.07038	0.96025	−0.13637	0.96559	−0.05555	0.10612	−0.04029	0.10911
15	50	−0.01530	0.73004	−0.10374	0.75929	−0.01214	0.09868	0.00178	0.09054
15	100	−0.03983	0.56330	−0.14048	0.60055	0.00124	0.09801	0.01643	0.07781

Table 4. *Monte Carlo comparison of nonparametric estimators of* $\xi J\left(T_{j,n}(t_1,t_2)\right)$ *and* $\mathrm{JCRJ}_{j,n}(t_1,t_2)$ *under Weibull* $(shape=1.3, scale=1.5)$ *components (double inspection at* $t_1=1$, $t_2=2$*).*

		CRJ				JCRJ			
		Plug-in		Kernel		Plug-in		Kernel	
n_{sys}	N_{sample}	Bias	RMSE	Bias	RMSE	Bias	RMSE	Bias	RMSE
5	20	−0.08999	0.31337	−0.05625	0.22000	0.00719	0.15384	0.00179	0.01662
5	30	−0.06331	0.20133	−0.05079	0.17457	0.00174	0.01589	0.00263	0.01324
5	50	−0.02523	0.13905	−0.02758	0.13062	0.00132	0.01337	0.00202	0.01085
5	100	−0.01954	0.09671	−0.02979	0.09502	0.00115	0.00853	0.00211	0.00764
7	20	−0.20823	1.33903	−0.07995	0.30672	0.00104	0.02984	0.00315	0.02623
7	30	−0.04657	0.23443	−0.04918	0.23071	0.00119	0.02260	0.00282	0.01977
7	50	−0.01938	0.17746	−0.03481	0.17741	0.00193	0.01807	0.00273	0.01534
7	100	−0.01699	0.12811	−0.03780	0.13045	0.00140	0.01229	0.00318	0.01133
10	20	−0.09480	0.98879	−0.05258	0.40438	−0.01568	0.03710	−0.00705	0.03501
10	30	−0.08285	0.73053	−0.07527	0.35265	−0.00502	0.03626	−0.00041	0.03217
10	50	−0.02678	0.27944	−0.06161	0.28291	0.00140	0.03569	0.00406	0.03192
10	100	−0.02813	0.19860	−0.06808	0.20556	0.00177	0.02483	0.00503	0.02320
15	20	0.10802	1.03245	0.07759	0.54276	−0.06746	0.06920	−0.04589	0.04882
15	30	0.06964	0.47126	−0.00642	0.48366	−0.05231	0.05976	−0.03410	0.04771
15	50	0.03628	0.39652	−0.02429	0.38982	−0.02633	0.05196	−0.01567	0.04269
15	100	−0.00021	0.30460	−0.06549	0.30756	−0.00167	0.05183	0.00446	0.04144

Downloaded from https://www.cambridge.org/core. UNIVERSIDAD AUTONOMA METROPOLITANA, on 17 Nov 2026 at 01:28:28, subject to the Cambridge Core terms of use, available at https://www.cambridge.org/core/terms. https://doi.org/10.1017/S0269964826100369

Table 5. *Monte Carlo comparison of nonparametric estimators of* $\xi J\big(T_{j,n}(t_1,t_2)\big)$ *and* $\mathrm{JCRJ}_{j,n}(t_1,t_2)$ *under EW components with CDF* $F(x) = \left(1-e^{-(x/\lambda)^\beta}\right)^\alpha$ *using* $(\alpha,\beta,\lambda) = (0.7, 1.3, 1.5)$ *(double inspection at* $t_1 = 1$, $t_2 = 2$*).*

		CRJ				JCRJ			
		Plug-in		Kernel		Plug-in		Kernel	
n_{sys}	N_{sample}	Bias	RMSE	Bias	RMSE	Bias	RMSE	Bias	RMSE
5	20	−0.19570	1.02952	−0.05711	0.21008	0.03743	0.36971	0.00086	0.01426
5	30	−0.13499	0.96665	−0.04370	0.17326	0.00943	0.16776	0.00234	0.01404
5	50	−0.03829	0.14206	−0.02886	0.12714	0.00133	0.01114	0.00169	0.00954
5	100	−0.02120	0.08960	−0.02059	0.08280	0.00072	0.00742	0.00124	0.00645
7	20	−0.60870	2.71738	−0.05839	0.27193	−0.00018	0.02889	0.00162	0.02397
7	30	−0.16578	1.15693	−0.05139	0.20351	0.00310	0.02318	0.00261	0.01765
7	50	−0.04991	0.17325	−0.04253	0.16113	0.00128	0.01329	0.00207	0.01203
7	100	−0.01630	0.12043	−0.02412	0.11544	0.00100	0.00959	0.00185	0.00866
10	20	−0.58864	2.62671	−0.10784	0.38553	−0.00456	0.02932	0.00016	0.02856
10	30	−0.09667	0.71337	−0.06170	0.28815	−0.00119	0.02530	0.00046	0.02219
10	50	−0.04832	0.22026	−0.05776	0.22112	0.00127	0.02153	0.00274	0.01836
10	100	−0.01029	0.15274	−0.02920	0.15649	−0.00011	0.01370	0.00160	0.01221
15	20	−0.16176	1.37047	−0.07890	0.51319	−0.03587	0.04013	−0.02104	0.03457
15	30	−0.09629	1.18492	−0.03078	0.43777	−0.02068	0.03734	−0.01126	0.03322
15	50	−0.02273	0.35417	−0.06000	0.36136	−0.00493	0.03721	−0.00068	0.02653
15	100	−0.01205	0.24569	−0.05862	0.25347	−0.00091	0.02753	0.00284	0.02604

diminishing RMSE as N increases, supports the use of the divergence estimator for structural comparison under inspection, even when n is moderately large. Overall, Table 4 confirms that in a regular hazard regime, both CRJ and JCRJ are accurately recoverable, and kernel smoothing mainly accelerates finite-sample stabilization.

Finally, we consider EW components with CDF

$$F(x) = \left(1-e^{-(x/\lambda)^\beta}\right)^\alpha, \qquad x > 0,$$

using $(\alpha,\beta,\lambda) = (0.7, 1.3, 1.5)$. Table 5 reports the results. Relative to the Weibull baseline, the CRJ plug-in RMSE is larger for small N in several settings, which is consistent with the additional shape flexibility induced by the exponentiation parameter α. Kernel smoothing produces a clear improvement for CRJ across most (n,N), confirming that smoothing is particularly valuable for stabilizing an absolute uncertainty functional that depends quadratically on the estimated conditional survival curve. For JCRJ, both estimators again remain stable and display decreasing RMSE with increasing N. The kernel estimator yields the most uniform performance across system sizes, indicating that smoothing also stabilizes the complexity estimator when the baseline model is more shape-flexible. Overall, Table 5 supports the conclusion that the proposed estimators remain reliable under flexible lifetime families, with kernel smoothing providing the strongest gains for CRJ.

Concluding remarks. Across Tables 3–5, RMSE decreases with N for both criteria, confirming the practical convergence of the proposed estimators under double inspection. Kernel smoothing is most beneficial for CRJ (uncertainty), particularly under heavier-tailed or more shape-flexible baselines, whereas JCRJ (complexity) is estimated stably across a wide range of (n,N) and provides a robust architecture-sensitive summary under periodic inspections.

Downloaded from https://www.cambridge.org/core. UNIVERSIDAD AUTONOMA METROPOLITANA, on 17 Nov 2026 at 01:28:28, subject to the Cambridge Core terms of use, available at https://www.cambridge.org/core/terms. https://doi.org/10.1017/S0269964826100369

5. Medical image analysis under double periodic inspection via CRJ and JCRJ

This section illustrates how the inspection-conditioned uncertainty and complexity functionals developed in Sections 2–4 can be operationalized in a digital imaging context. A key methodological point is that the image is not treated merely as a histogram. Instead, the double periodic inspection mechanism is embedded directly into the analysis by interpreting normalized pixel intensities as realizations from an unknown baseline CDF F supported on $[0,1]$. Two inspection thresholds $0 < t_1 < t_2 < 1$ act as information gates that generate the inspection event

$$t_1 < X_{j:n} < t_2 < T(n),$$

and therefore induce the conditional residual structure quantified by $\xi J\big(T_{j,n}(t_1,t_2)\big)$ and $\mathrm{JCRJ}_{j,n}(t_1,t_2)$. In this way, the uncertainty score is compelled to respect the same two-stage observation protocol that drives the reliability model of the paper.

We use a publicly available brain MRI slice from Wikimedia Commons. Specifically, X denotes a grayscale MRI image downloaded from the Wikimedia Commons file
https://upload.wikimedia.org/wikipedia/commons/b/b2/MRI_of_Human_Brain.jpg.

The image is used here solely as a representative medical texture with heterogeneous regions (high-contrast outer boundary, mid-gray tissues, and low-intensity background). The usage and redistribution terms are governed by the license stated on the corresponding Wikimedia Commons source page.

Let the normalized grayscale image be $X \in [0,1]$, obtained by affine rescaling of the pixel values to the unit interval. To probe sensitivity to clinically relevant photometric manipulations (e.g., window/level changes), we construct three deterministic perturbations:

$$Y = \mathrm{rescale}(0.92X + 0.04)\,, \qquad Z = \mathrm{rescale}\Big(X^{1.8}\Big)\,, \qquad W = \mathrm{rescale}\Big(X^{0.55}\Big)\,,$$

where $\mathrm{rescale}(\cdot)$ denotes a min–max renormalization to $[0,1]$ applied after each transformation. This implementation detail preserves dynamic range and avoids degenerate near-binary images that can arise when power transformations are applied directly on already low-contrast medical scans. The linear map in Y mimics a mild contrast/brightness adjustment; the convex map Z emphasizes bright structures and suppresses mid-tones; and the concave map W expands low intensities and compresses high intensities.

To ensure that both uncertainty (CRJ) and structural complexity (JCRJ) are nondegenerate and signature-sensitive, we evaluate the image-derived indices under two distinct coherent-system signatures, consistent with the double inspection model of this paper:

- **Architecture A (two-point tail signature).** We take $n = 10$ and

$$\boldsymbol{s}^{(A)} = (0,\ldots,0,\tfrac{1}{2},\tfrac{1}{2}), \qquad i = n-1, \qquad j = n-2,$$

  so that only the last two order-statistic failure modes contribute to the conditional mixture under double inspection.
- **Architecture B (four-component hybrid signature).** We take $n = 4$ and

$$\boldsymbol{s}^{(B)} = \Big(0,\tfrac{1}{6},\tfrac{7}{12},\tfrac{1}{4}\Big), \qquad i = 2, \qquad j = 1,$$

  which belongs to the four-component coherent class studied earlier and induces a richer inspection-dependent mixture.

For the empirical implementation, we randomly sample $N = 5,000$ pixel intensities from the normalized MRI image without imposing any spatial model, and we apply the same deterministic transformations to obtain the samples associated with Y, Z, and W. Thus, the four channels are analyzed on a common

Downloaded from https://www.cambridge.org/core. UNIVERSIDAD AUTONOMA METROPOLITANA, on 17 Nov 2026 at 01:28:28, subject to the Cambridge Core terms of use, available at https://www.cambridge.org/core/terms. https://doi.org/10.1017/S0269964826100369

sampled intensity basis, which makes the resulting CRJ and JCRJ comparisons directly interpretable as consequences of the photometric transformations rather than of unequal sample sizes.

We fix the first inspection threshold at $t_1 = 0.35$ and evaluate the second inspection threshold over a grid $t_2 \in \{0.45, 0.50, \ldots, 0.80\}$, always enforcing $t_2 > t_1$. For each image (X, Y, Z, W), we compute: (i) a plug-in estimator obtained by substituting the empirical CDF $\widehat{F}_N$ into the closed-form expressions of $p_k(j, t_1, t_2)$ and $\nu_{k,j}(t_1, t_2, \cdot)$ and (ii) a kernel-smoothed estimator obtained by replacing $\widehat{F}_N$ with $\widehat{F}_{N,h}$. The resulting estimated conditional SF $\widehat{F}_{T_{j,n}(t_1,t_2)}(x)$ is then inserted into the quadratic functionals defining CRJ and JCRJ.

To address empirical variability, we complement the point estimates with percentile bootstrap uncertainty quantification. For each image channel and each architecture, we generate $B = 200$ bootstrap resamples, recompute both the plug-in and kernel estimators, and then report pointwise 95% bootstrap confidence intervals together with bootstrap standard errors along the entire t_2 grid. Because the paper does not derive closed-form variance expressions or asymptotic laws for these nonlinear functionals, the bootstrap is used here as a practical finite-sample device for uncertainty assessment rather than as a substitute for a full asymptotic distribution theory.

The two indices play complementary roles:

- CRJ is an absolute uncertainty index under double inspection; values closer to 0 indicate lower conditional uncertainty in the inspection-conditioned residual structure.
- JCRJ is a relative structural complexity index; larger values indicate greater divergence between the conditional system residual lifetime and its signature-weighted conditional components, hence stronger architectural heterogeneity.

Figure 9 displays the benchmark MRI image and its three deterministic perturbations generated exactly as in the computational pipeline. The CRJ and JCRJ trajectories, together with their bootstrap confidence bands, are reported in Figures 10–13. This resolves the cross-reference issue in the earlier version by explicitly pointing to the empirical figures used in the discussion below.

We now quantify how the proposed inspection-conditioned indices discriminate among the benchmark brain MRI image X and its deterministic photometric perturbations $Y = \text{rescale}(0.92X + 0.04)$, $Z = \text{rescale}(X^{1.8})$, and $W = \text{rescale}(X^{0.55})$ (Figure 9). Throughout, we interpret normalized pixel intensities as an IID sample from an unknown baseline distribution F supported on $[0, 1]$ and impose the double periodic inspection mechanism through two thresholds $0 < t_1 < t_2 < 1$. We fix $t_1 = 0.35$ and vary the second inspection threshold over the grid $t_2 \in \{0.45, 0.50, \ldots, 0.80\}$. For each t_2, we evaluate the inspection-conditioned residual lifetime $T_{j,n}(t_1, t_2)$ under the two architectures defined above.

Figures 10–13 report not only the estimated CRJ and JCRJ curves but also the associated pointwise 95% bootstrap confidence bands for both the plug-in and kernel procedures. This additional layer is important for the empirical application because it shows which features of the trajectories are stable under resampling and which are potentially sensitive to finite-sample fluctuation. Across all panels, the plug-in and kernel curves remain very close, and their confidence bands overlap substantially, indicating that the main conclusions are not driven by the particular nonparametric smoothing device.

Across all channels and both architectures, the estimated CRJ profiles exhibit a clear and systematic dependence on the second inspection threshold. In the present implementation, the CRJ curves move monotonically downward as t_2 increases, so the conditional uncertainty profile is not flat with respect to the inspection horizon. This monotone behavior is consistently reproduced by the bootstrap replications, and the confidence bands typically become narrower for larger t_2, reflecting reduced empirical variability in the later-inspection regime. The effect is visible for both the plug-in and kernel estimators and therefore appears to be structurally linked to the inspection-conditioning mechanism rather than to a particular estimation scheme.

The numerical output confirms that the two estimators are nearly indistinguishable in magnitude. For example, under Architecture A and for the original image X at $t_2 = 0.60$, the plug-in estimate of CRJ is approximately -2.433 with a 95% bootstrap confidence interval $(-2.441, -2.426)$,

Downloaded from https://www.cambridge.org/core. UNIVERSIDAD AUTONOMA METROPOLITANA, on 17 Nov 2026 at 01:28:28, subject to the Cambridge Core terms of use, available at https://www.cambridge.org/core/terms. https://doi.org/10.1017/S0269964826100369

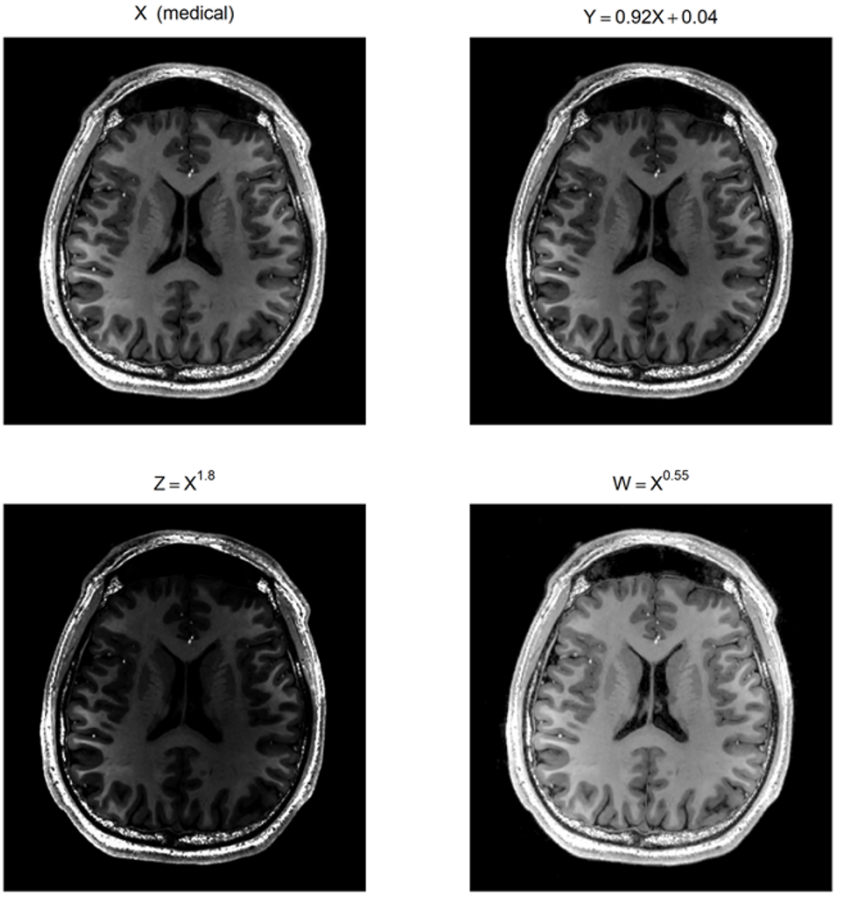


Figure 9. *Benchmark medical image X (brain MRI slice) and its deterministic photometric perturbations generated in the numerical pipeline:* $Y = \text{rescale}(0.92X + 0.04)$, $Z = \text{rescale}(X^{1.8})$, *and* $W = \text{rescale}(X^{0.55})$, *where* rescale *denotes min–max normalization to* $[0, 1]$.

while the corresponding JCRJ estimate is about 0.0010 with interval $(0.0008, 0.0011)$. Under Architecture B for the same image and threshold, the plug-in CRJ estimate is approximately -2.420 with interval $(-2.427, -2.411)$, whereas the JCRJ estimate is approximately -0.0096 with interval $(-0.0106, -0.0084)$. These representative values illustrate two points simultaneously: first, the empirical uncertainty bands are fairly tight, and second, the inferential scale of JCRJ can depend materially on the system architecture.

Beyond this global pattern, the CRJ trajectories still discriminate meaningfully among the four image channels. The benchmark image X and the mild affine perturbation Y remain very close throughout, with strong overlap of their confidence bands, showing that a modest brightness/contrast adjustment does not substantially alter the inspection-conditioned residual uncertainty. By contrast, the nonlinear transforms Z and W produce visibly different CRJ trajectories, indicating that convex and concave remappings of intensities modify the residual structure seen through the double-inspection filter. Hence, the method is able to separate photometric changes that are essentially distribution-preserving from those that materially reshape the inspection-conditioned uncertainty profile.

The JCRJ results provide complementary information by focusing on complexity induced by the signature-weighted conditional mixture. Here again, the bootstrap bands are informative. They show that the major ranking patterns are stable, while also clarifying where channel-specific differences become small enough that over-interpretation should be avoided. In particular, the uncertainty ribbons tend

Downloaded from https://www.cambridge.org/core. UNIVERSIDAD AUTONOMA METROPOLITANA, on 17 Nov 2026 at 01:28:28, subject to the Cambridge Core terms of use, available at https://www.cambridge.org/core/terms. https://doi.org/10.1017/S0269964826100369

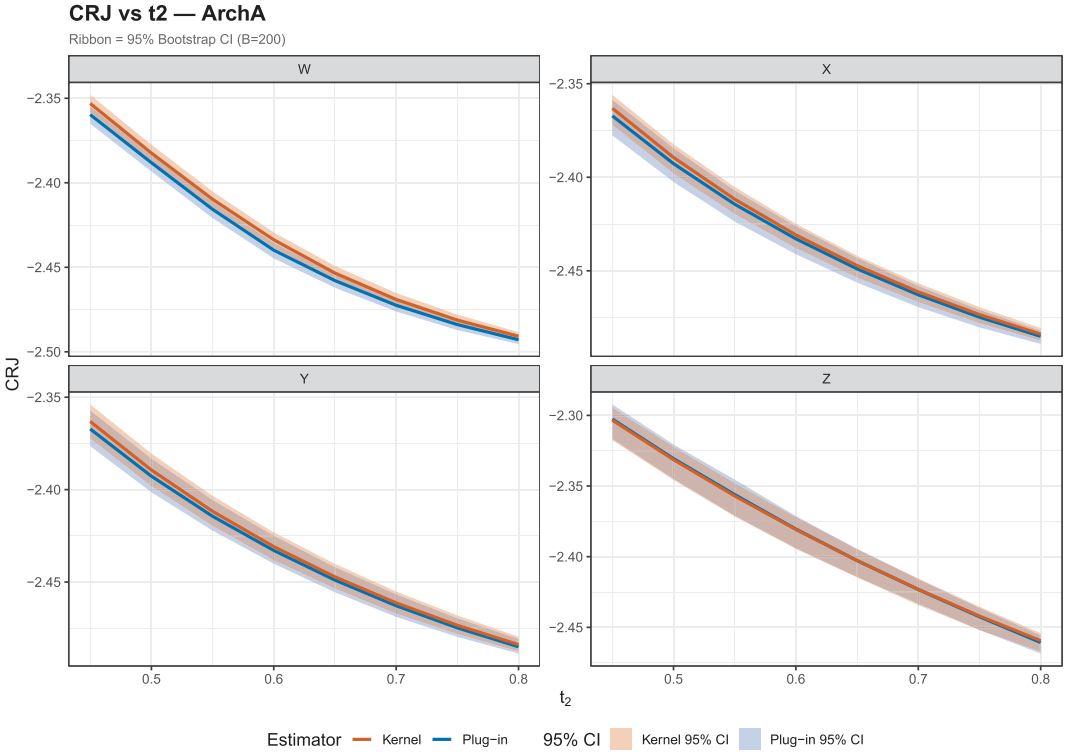


Figure 10. *CRJ trajectories for Architecture A with pointwise* 95% *bootstrap confidence bands* ($B = 200$) *under the plug-in and kernel estimators, for* $t_1 = 0.35$ *and* $t_2 \in \{0.45, 0.50, \ldots, 0.80\}$.

to be wider for smaller t_2 and narrower for larger t_2, which is consistent with the visual impression that early-inspection complexity is more sensitive to finite-sample fluctuation. At the substantive level, JCRJ distinguishes how the image transformation interacts with the architecture of the coherent system. Architectures A and B do not simply rescale one another; rather, they emphasize different inspection-conditioned component mixtures, so the same transformation can display different complexity behavior under the two signatures. This is precisely the type of architecture-sensitive effect that JCRJ is designed to capture.

From the standpoint of medical-image analysis, the contribution of the proposed framework is therefore not merely to produce another set of intensity summaries. Instead, CRJ and JCRJ supply two complementary descriptors of the image intensity field under a prescribed inspection protocol: CRJ measures inspection-conditioned residual uncertainty, while JCRJ measures inspection-conditioned mixture complexity. In practical terms, this allows one to compare whether a transformation primarily changes the overall uncertainty of the residual intensity structure, the architecture-sensitive heterogeneity of that structure, or both. The MRI example shows that these two aspects need not move in lockstep, which is useful when assessing the effect of clinically relevant preprocessing operations such as contrast adjustment or nonlinear intensity remapping.

More broadly, the empirical application now supports three concrete messages. First, the method is stable: the plug-in and kernel implementations lead to almost identical trajectories and heavily overlapping confidence bands. Second, the method is discriminative: it separates the original image and the mild affine perturbation from the more structurally disruptive nonlinear transforms. Third, the method is uncertainty-aware: by reporting bootstrap confidence intervals and bootstrap standard errors, the revised analysis no longer relies on point estimates alone. This directly addresses the reviewer concern that the earlier version lacked variability assessment in the applied section.

Downloaded from https://www.cambridge.org/core. UNIVERSIDAD AUTONOMA METROPOLITANA, on 17 Nov 2026 at 01:28:28, subject to the Cambridge Core terms of use, available at https://www.cambridge.org/core/terms. https://doi.org/10.1017/S0269964826100369

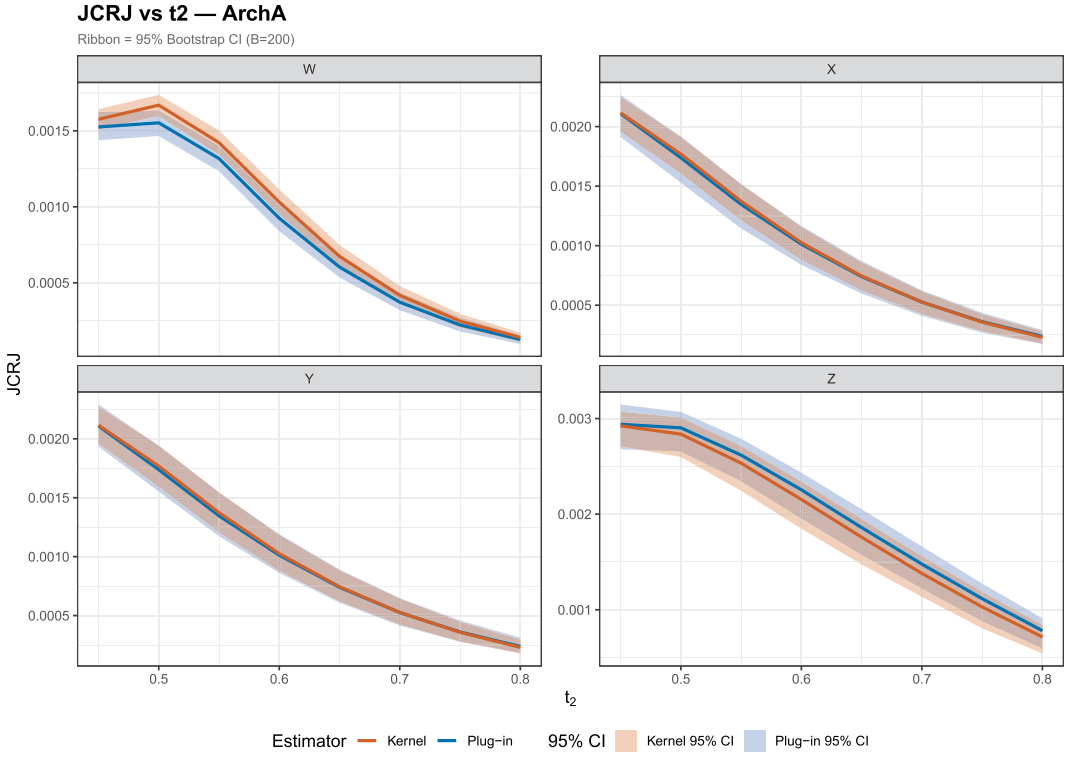


Figure 11. *JCRJ trajectories for Architecture A with pointwise* 95% *bootstrap confidence bands (*$B = 200$*) under the plug-in and kernel estimators, for* $t_1 = 0.35$ *and* $t_2 \in \{0.45, 0.50, \ldots, 0.80\}$.

Taken together, Figures 10–13 show that the proposed inspection-conditioned functionals are empirically informative and practically interpretable. They reveal not only how the estimated CRJ and JCRJ curves behave across inspection thresholds, but also how reliable those estimated trajectories are under resampling. Accordingly, the medical-image example now serves a dual purpose: it illustrates the applied meaning of the proposed nonparametric estimators and, at the same time, documents their finite-sample stability in a realistic imaging setting.

To complement the graphical presentation, Tables 6–9 report the point estimates, bootstrap standard errors, and pointwise 95% bootstrap confidence intervals for the plug-in estimator at all inspection thresholds. We report the plug-in tables in the main text for compactness, since the kernel-based results are numerically very close and visually overlap with the plug-in bands in the figures. The full kernel numerical results are available in the supplementary computational output.

Several points emerge from Tables 6–9. First, the bootstrap standard errors are small relative to the magnitude of the corresponding estimates in nearly all settings, which provides direct numerical support for the stability suggested by the smooth curves in Figures 10–13. Second, the confidence intervals for X and Y are almost indistinguishable throughout much of the threshold grid, under both architectures and for both measures. This numerical overlap strengthens the interpretation that a mild affine intensity transformation leaves the inspection-conditioned complexity structure largely intact. Third, the nonlinear channels Z and W exhibit more noticeable separation in both point estimates and confidence intervals, especially for JCRJ under Architecture B, where the threshold-dependent transition from positive to negative values is clearly resolved. A further recurring feature is the reduction in uncertainty as t_2 increases. In both architectures, and for both CRJ and JCRJ, the bootstrap standard errors and the widths of the confidence intervals tend to decrease in the upper-threshold regime. This trend is also consistent with the visual impression of tighter overlap in the graphical displays at larger values

Downloaded from https://www.cambridge.org/core. UNIVERSIDAD AUTONOMA METROPOLITANA, on 17 Nov 2026 at 01:28:28, subject to the Cambridge Core terms of use, available at https://www.cambridge.org/core/terms. https://doi.org/10.1017/S0269964826100369

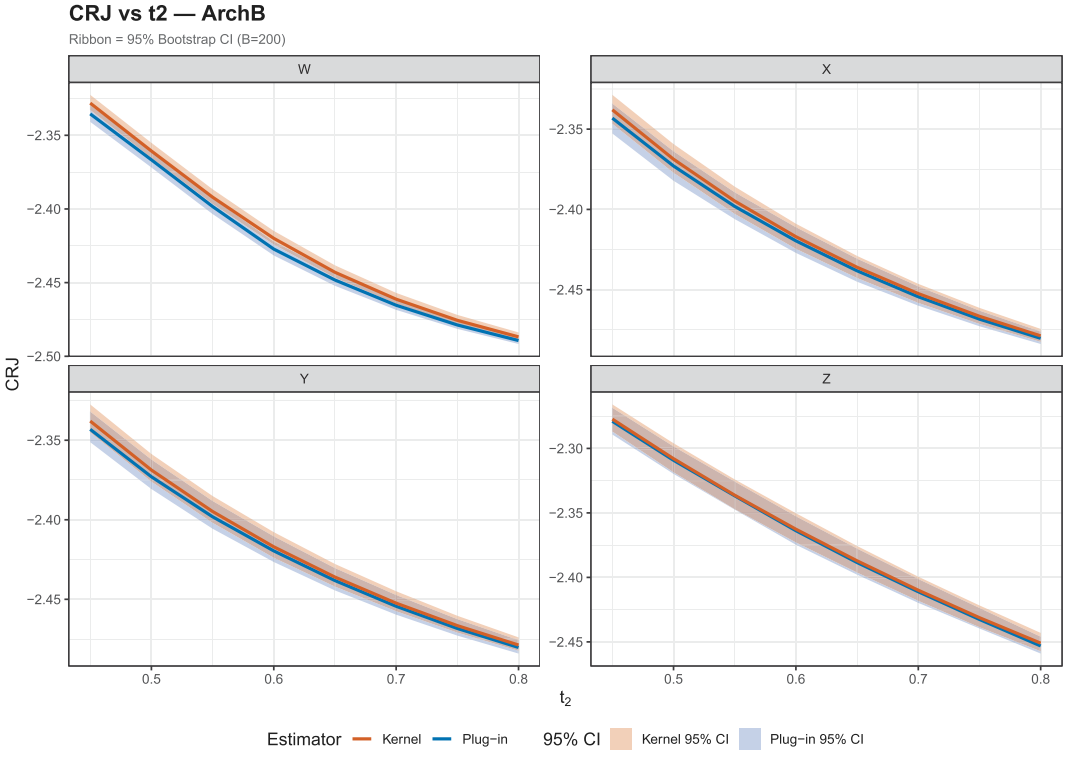


Figure 12. *CRJ trajectories for Architecture B with pointwise* 95% *bootstrap confidence bands (*$B = 200$*) under the plug-in and kernel estimators, for* $t_1 = 0.35$ *and* $t_2 \in \{0.45, 0.50, \ldots, 0.80\}$.

of t_2. From an applied perspective, this means that the proposed estimators are not only able to detect meaningful differences between channels but also become increasingly stable in the higher-threshold inspection range. Taken together, the image panels, the threshold-dependent curves, and the numerical uncertainty summaries lead to a coherent practical conclusion. The proposed CRJ and JCRJ measures behave conservatively under the mild affine modification Y but respond clearly to the nonlinear transformations Z and W. This is precisely the pattern one would hope to see from a useful complexity descriptor in medical image analysis: it should not overreact to benign distribution-preserving perturbations, yet it should register deeper structural alterations when they are present. Moreover, the comparison between Architectures A and B shows that the framework is sensitive to architecture-dependent changes in image organization, thereby extending its relevance beyond a single processing configuration. Overall, these findings support the use of CRJ and JCRJ as stable and practically informative nonparametric tools for comparing transformed medical images under inspection-conditioned uncertainty.

For full transparency and reproducibility, the analysis code (including image preprocessing, computation of CRJ and JCRJ, bootstrap uncertainty quantification, and figure generation) is publicly available at the following GitHub repository: https://github.com/rezaalizadehn/Noughabi. This repository enables full replication of the results and facilitates further use of the proposed methodology by other researchers.

6. Conclusion and broader significance

Periodic inspections fundamentally reshape reliability analysis because remaining lifetime must be evaluated conditionally on partial evidence revealed at inspection times. In this work, we developed

Downloaded from https://www.cambridge.org/core. UNIVERSIDAD AUTONOMA METROPOLITANA, on 17 Nov 2026 at 01:28:28, subject to the Cambridge Core terms of use, available at https://www.cambridge.org/core/terms. https://doi.org/10.1017/S0269964826100369

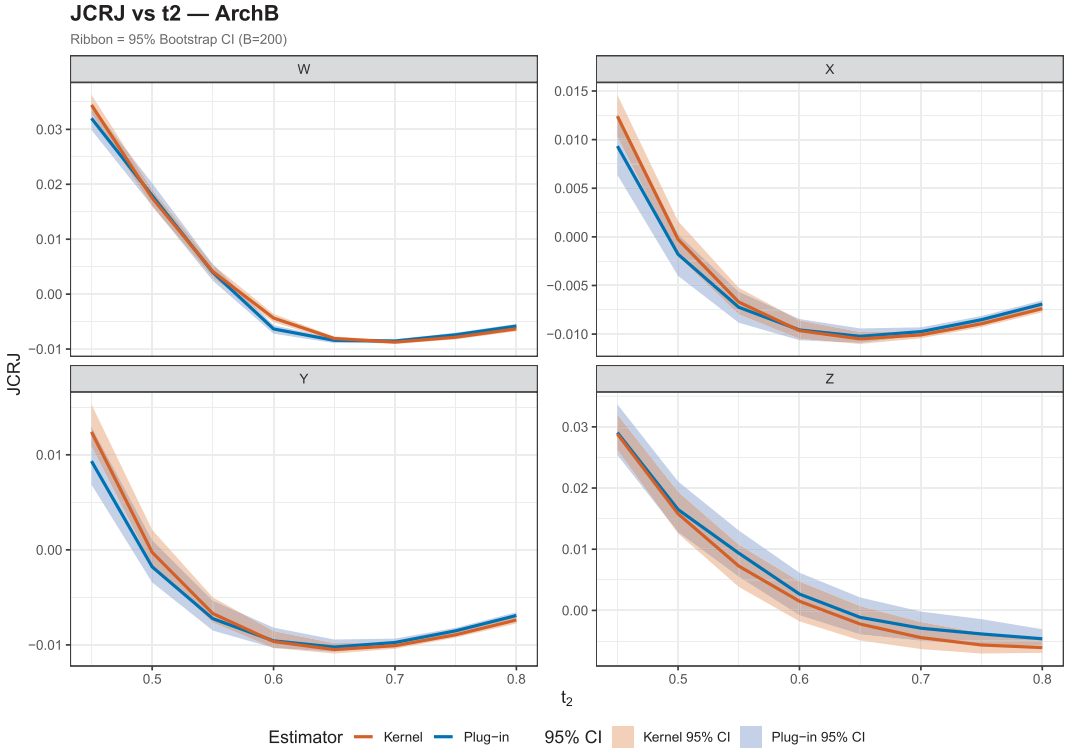


Figure 13. *JCRJ trajectories for Architecture B with pointwise* 95% *bootstrap confidence bands (B =* 200*) under the plug-in and kernel estimators, for* $t_1 = 0.35$ *and* $t_2 \in \{0.45, 0.50, \ldots, 0.80\}$.

Table 6. *Architecture A: CRJ plug-in estimates with bootstrap standard errors and pointwise* 95% *bootstrap confidence intervals.*

Channel	t_2	Estimate	SE	95% CI lower	95% CI upper
X	0.45	−2.367189	0.004967	−2.377601	−2.358493
X	0.50	−2.392735	0.004695	−2.402494	−2.384432
X	0.55	−2.414421	0.004359	−2.423657	−2.406982
X	0.60	−2.432915	0.003936	−2.441119	−2.426149
X	0.65	−2.448964	0.003468	−2.456300	−2.443004
X	0.70	−2.462835	0.002943	−2.469409	−2.458024
X	0.75	−2.474803	0.002420	−2.480259	−2.470840
X	0.80	−2.485031	0.001899	−2.489116	−2.481955
Y	0.45	−2.367189	0.004869	−2.376480	−2.357116
Y	0.50	−2.392735	0.004626	−2.401407	−2.383133
Y	0.55	−2.414421	0.004295	−2.422188	−2.405554
Y	0.60	−2.432915	0.003918	−2.440084	−2.424935
Y	0.65	−2.448964	0.003488	−2.455527	−2.441901
Y	0.70	−2.462835	0.002998	−2.468847	−2.456617
Y	0.75	−2.474803	0.002490	−2.479663	−2.469526
Y	0.80	−2.485031	0.001967	−2.488701	−2.480711

(*Continued*)

Downloaded from https://www.cambridge.org/core. UNIVERSIDAD AUTONOMA METROPOLITANA, on 17 Nov 2026 at 01:28:28, subject to the Cambridge Core terms of use, available at https://www.cambridge.org/core/terms. https://doi.org/10.1017/S0269964826100369

Table 6. *(Continued.)*

Channel	t_2	Estimate	SE	95% CI lower	95% CI upper
Z	0.45	−2.302610	0.005987	−2.316744	−2.292254
Z	0.50	−2.330604	0.006060	−2.345059	−2.320606
Z	0.55	−2.356051	0.005905	−2.371081	−2.345471
Z	0.60	−2.380469	0.005617	−2.394043	−2.371202
Z	0.65	−2.402761	0.005208	−2.414456	−2.394641
Z	0.70	−2.423224	0.004613	−2.433345	−2.415734
Z	0.75	−2.442514	0.003961	−2.451847	−2.436267
Z	0.80	−2.460719	0.003245	−2.468539	−2.455519
W	0.45	−2.359671	0.002938	−2.365083	−2.354686
W	0.50	−2.388117	0.002887	−2.393309	−2.383249
W	0.55	−2.415693	0.002792	−2.420865	−2.410962
W	0.60	−2.439858	0.002580	−2.444740	−2.435421
W	0.65	−2.457894	0.002308	−2.462088	−2.453818
W	0.70	−2.472484	0.001966	−2.476143	−2.468732
W	0.75	−2.483891	0.001626	−2.487141	−2.480713
W	0.80	−2.492871	0.001253	−2.495366	−2.490648

Table 7. *Architecture A: JCRJ plug-in estimates with bootstrap standard errors and pointwise* 95% *bootstrap confidence intervals.*

Channel	t_2	Estimate	SE	95% CI lower	95% CI upper
X	0.45	0.002109	0.000093	0.001912	0.002267
X	0.50	0.001738	0.000100	0.001529	0.001915
X	0.55	0.001347	0.000096	0.001143	0.001516
X	0.60	0.001012	0.000085	0.000839	0.001166
X	0.65	0.000740	0.000071	0.000598	0.000870
X	0.70	0.000526	0.000057	0.000411	0.000624
X	0.75	0.000361	0.000043	0.000269	0.000436
X	0.80	0.000238	0.000031	0.000174	0.000290
Y	0.45	0.002109	0.000091	0.001935	0.002292
Y	0.50	0.001738	0.000098	0.001552	0.001942
Y	0.55	0.001347	0.000094	0.001173	0.001546
Y	0.60	0.001012	0.000085	0.000863	0.001191
Y	0.65	0.000740	0.000072	0.000609	0.000891
Y	0.70	0.000526	0.000058	0.000415	0.000648
Y	0.75	0.000361	0.000045	0.000279	0.000458
Y	0.80	0.000238	0.000032	0.000182	0.000313
Z	0.45	0.002940	0.000116	0.002680	0.003148
Z	0.50	0.002903	0.000101	0.002653	0.003069
Z	0.55	0.002618	0.000111	0.002343	0.002790
Z	0.60	0.002255	0.000122	0.001952	0.002434
Z	0.65	0.001860	0.000123	0.001572	0.002052

(*Continued*)

Downloaded from https://www.cambridge.org/core. UNIVERSIDAD AUTONOMA METROPOLITANA, on 17 Nov 2026 at 01:28:28, subject to the Cambridge Core terms of use , available at https://www.cambridge.org/core/terms. https://doi.org/10.1017/S0269964826100369

Table 7. *(Continued.)*

Channel	t_2	Estimate	SE	95% CI lower	95% CI upper
Z	0.70	0.001478	0.000114	0.001221	0.001662
Z	0.75	0.001116	0.000100	0.000879	0.001274
Z	0.80	0.000781	0.000082	0.000594	0.000911
W	0.45	0.001525	0.000047	0.001438	0.001623
W	0.50	0.001553	0.000043	0.001466	0.001635
W	0.55	0.001318	0.000049	0.001234	0.001402
W	0.60	0.000925	0.000049	0.000840	0.001012
W	0.65	0.000604	0.000042	0.000536	0.000677
W	0.70	0.000373	0.000032	0.000320	0.000437
W	0.75	0.000223	0.000023	0.000180	0.000272
W	0.80	0.000127	0.000015	0.000098	0.000156

Table 8. *Architecture B: CRJ plug-in estimates with bootstrap standard errors and pointwise* 95% *bootstrap confidence intervals.*

Channel	t_2	Estimate	SE	95% CI lower	95% CI upper
X	0.45	−2.343140	0.004800	−2.352710	−2.334097
X	0.50	−2.372956	0.004643	−2.382126	−2.363814
X	0.55	−2.398121	0.004366	−2.406018	−2.389352
X	0.60	−2.419573	0.004028	−2.427081	−2.411101
X	0.65	−2.438235	0.003607	−2.445020	−2.430698
X	0.70	−2.454389	0.003116	−2.459935	−2.447936
X	0.75	−2.468329	0.002595	−2.472757	−2.463059
X	0.80	−2.480269	0.002075	−2.483794	−2.476077
Y	0.45	−2.343140	0.004877	−2.351224	−2.331990
Y	0.50	−2.372956	0.004740	−2.380668	−2.362166
Y	0.55	−2.398121	0.004468	−2.405626	−2.388196
Y	0.60	−2.419573	0.004084	−2.426536	−2.410450
Y	0.65	−2.438235	0.003646	−2.444416	−2.430386
Y	0.70	−2.454389	0.003160	−2.459655	−2.447308
Y	0.75	−2.468329	0.002637	−2.472816	−2.462484
Y	0.80	−2.480269	0.002082	−2.484104	−2.475697
Z	0.45	−2.278978	0.004992	−2.289210	−2.268518
Z	0.50	−2.309204	0.005300	−2.319715	−2.298480
Z	0.55	−2.336758	0.005348	−2.347445	−2.325731
Z	0.60	−2.363778	0.005269	−2.374679	−2.352637
Z	0.65	−2.388480	0.004976	−2.397869	−2.377686
Z	0.70	−2.411140	0.004547	−2.419752	−2.401285
Z	0.75	−2.432599	0.004018	−2.439610	−2.423715
Z	0.80	−2.453134	0.003392	−2.459036	−2.445972
W	0.45	−2.335456	0.002788	−2.340870	−2.329487
W	0.50	−2.366643	0.002758	−2.371839	−2.360642

(*Continued*)

Downloaded from https://www.cambridge.org/core. UNIVERSIDAD AUTONOMA METROPOLITANA, on 17 Nov 2026 at 01:28:28, subject to the Cambridge Core terms of use, available at https://www.cambridge.org/core/terms. https://doi.org/10.1017/S0269964826100369

Table 8. *(Continued.)*

Channel	t_2	Estimate	SE	95% CI lower	95% CI upper
W	0.55	−2.398335	0.002630	−2.403421	−2.392528
W	0.60	−2.427238	0.002434	−2.431542	−2.422103
W	0.65	−2.448242	0.002211	−2.452150	−2.443292
W	0.70	−2.465347	0.001927	−2.468484	−2.461072
W	0.75	−2.478743	0.001618	−2.481383	−2.475049
W	0.80	−2.489311	0.001304	−2.491639	−2.486410

Table 9. *Architecture B: JCRJ plug-in estimates with bootstrap standard errors and pointwise* 95% *bootstrap confidence intervals.*

Channel	t_2	Estimate	SE	95% CI lower	95% CI upper
X	0.45	0.009334	0.001566	0.006373	0.012610
X	0.50	−0.001792	0.001155	−0.004016	0.000289
X	0.55	−0.007244	0.000801	−0.008828	−0.005629
X	0.60	−0.009573	0.000581	−0.010631	−0.008452
X	0.65	−0.010229	0.000374	−0.010915	−0.009420
X	0.70	−0.009747	0.000217	−0.010132	−0.009309
X	0.75	−0.008519	0.000178	−0.008839	−0.008138
X	0.80	−0.006908	0.000185	−0.007229	−0.006530
Y	0.45	0.009334	0.001510	0.006860	0.012966
Y	0.50	−0.001792	0.001167	−0.003427	0.001035
Y	0.55	−0.007244	0.000845	−0.008495	−0.005344
Y	0.60	−0.009573	0.000596	−0.010320	−0.008189
Y	0.65	−0.010229	0.000354	−0.010733	−0.009434
Y	0.70	−0.009747	0.000195	−0.010086	−0.009341
Y	0.75	−0.008519	0.000152	−0.008776	−0.008205
Y	0.80	−0.006908	0.000166	−0.007204	−0.006567
Z	0.45	0.029063	0.002072	0.025405	0.033665
Z	0.50	0.016488	0.002130	0.012790	0.021067
Z	0.55	0.009362	0.001990	0.005487	0.013056
Z	0.60	0.002671	0.001741	−0.000809	0.006159
Z	0.65	−0.001134	0.001500	−0.003930	0.002118
Z	0.70	−0.002905	0.001255	−0.004985	−0.000192
Z	0.75	−0.003849	0.000986	−0.005574	−0.001430
Z	0.80	−0.004636	0.000678	−0.005748	−0.003076
W	0.45	0.032015	0.001224	0.029875	0.034437
W	0.50	0.017941	0.001097	0.016055	0.020196
W	0.55	0.003957	0.000773	0.002435	0.005449
W	0.60	−0.006342	0.000407	−0.007199	−0.005669
W	0.65	−0.008419	0.000230	−0.008914	−0.008017
W	0.70	−0.008540	0.000183	−0.008921	−0.008230
W	0.75	−0.007411	0.000196	−0.007823	−0.007027
W	0.80	−0.005819	0.000204	−0.006281	−0.005437

Downloaded from https://www.cambridge.org/core. UNIVERSIDAD AUTONOMA METROPOLITANA, on 17 Nov 2026 at 01:28:28, subject to the Cambridge Core terms of use , available at https://www.cambridge.org/core/terms. https://doi.org/10.1017/S0269964826100369

a signature-based information-theoretic framework for coherent systems under two scheduled inspections, with the conditional residual lifetime beyond the second inspection as the primary inferential target. By embedding the inspection-conditioned mixture structure into CRJ, we obtained an uncertainty index that is both structurally interpretable and operationally relevant: it responds directly to inspection timing and to redundancy allocation encoded by the system signature.

Our theoretical contributions are fourfold. First, we derived a signature-based representation of the inspection-conditioned CRJ that makes the joint role of system architecture and inspection timing explicit. Second, we established stochastic-order comparison results, under the usual, hazard-rate, and likelihood-ratio orders (Theorems 1 and 2), which provide rigorous ranking tools for conditional residual lifetimes and for the inspection-induced mixing structure, enabling transparent comparisons across coherent designs under a common inspection policy. Third, we introduced divergence measures built from CRJ that separate uncertainty magnitude from architecture-driven heterogeneity, yielding a principled notion of inspection-conditioned structural complexity. Fourth, on the inferential side, our nonparametric plug-in and kernel-smoothed estimators (Theorems 3 and 4) make the framework operational when the baseline lifetime distribution is unknown, being strongly consistent and consistent in probability, respectively.

From a practical standpoint, the framework equips reliability analysts and system designers with inspection-aware tools for comparing coherent architectures beyond unconditional reliability summaries, explicitly balancing uncertainty reduction against structural complexity under fixed inspection resources. Our numerical study makes these implications concrete. Example 1 shows how the underlying hazard regime, constant, increasing, or decreasing, together with the placement of the two inspection times jointly reshapes the CRJ profile, so that uncertainty contraction is governed not by inspection timing alone but by its interaction with component aging. Example 4 illustrates how the ordering results of Theorems 1–2 translate into a visible dominance of one system over another across the inspection plane, confirming that the stochastic-order criteria are not merely formal but yield actionable design rankings. The Monte Carlo results further indicate that both estimators perform reliably at realistic sample sizes.

Beyond classical reliability settings, the medical imaging study illustrates that the proposed inspection-conditioned indices are not tied to a specific engineering domain: when the same two-inspection protocol is imposed on normalized intensity distributions, the resulting uncertainty and complexity profiles can discriminate between photometric transformations in a manner consistent with their redistribution of mass across the intensity scale. This highlights a broader principle of the paper: once a two-stage observation protocol induces conditional residual structure, the proposed information measures provide a unified language for quantifying how evidence reduces uncertainty and how structure generates heterogeneity. Future work may extend these ideas to heterogeneous or dependent component lifetimes, to adaptive or optimized inspection schedules, and to alternative survival-based information functionals, further strengthening the link between information theory, inference under partial observation, and reliability-driven design. While the current work focuses on complete data, the proposed CRJ and JCRJ measures can, in principle, be adapted to interval-censored settings by replacing the empirical $\hat{F}$ with a suitable estimator for the SF under censoring. This extension represents a promising direction for future research.

Acknowledgments. The medical image used in Section 5 (brain MRI slice) was obtained from Wikimedia Commons and is publicly available at: https://upload.wikimedia.org/wikipedia/commons/7/71/MRI_of_Human_Brain.jpg. The image is distributed under the license specified on its corresponding Wikimedia Commons source page. No additional datasets were generated. R. Alizadeh Noughabi and Z. Pakdaman jointly developed the main theoretical framework, derived the mathematical results, and performed the analytical proofs. Both authors contributed equally to the writing of the manuscript, preparation of figures and numerical illustrations, and interpretation of the results. All authors reviewed and approved the final version of the manuscript. Both authors contributed equally to this work.

Funding statement. No funding was received for conducting this study.

Competing interest. The authors declare no competing interests.

Downloaded from https://www.cambridge.org/core. UNIVERSIDAD AUTONOMA METROPOLITANA, on 17 Nov 2026 at 01:28:28, subject to the Cambridge Core terms of use, available at https://www.cambridge.org/core/terms. https://doi.org/10.1017/S0269964826100369

References

[1] Alizadeh Noughabi R., Pakdaman Z., & Alizadeh Noughabi, H. (2026). A study of the complexity of conditional mixed systems and their duals with gamma components using the Jensen cumulative residual extropy divergence index. *Journal of Statistical Sciences* 20(1): 0–0.

[2] Arnold, B.C., Balakrishnan, N., & Nagaraja, H.N. (1992). *A First Course in Order Statistics.* New York: John Wiley and Sons.

[3] Asadi, M., & Bayramoglu, I. (2006). The mean residual life function of a *k*-out-of-*n* structure at the system level. *IEEE Transactions on Reliability* **55**(2): 314–318.

[4] Asadi, M., & Berred, A. (2025). The mean residual life at random age and its connection to variability measures. *Probability in the Engineering and Informational Sciences* **39**(3): 326–343.

[5] Asadi, M., Ebrahimi, N., Soofi, E.S., & Zohrevand, Y. (2016). Jensen–Shannon information of the coherent system lifetime. *Reliability Engineering & System Safety* **156**: 244–255.

[6] Asadi, M., & Goliforushani, S. (2008). On the mean residual life function of coherent systems. *IEEE Transactions on Reliability* **57**(4): 574–580.

[7] Barlow, R.E., & Proschan, F. (1975). *Statistical Theory of Reliability and Life Testing: Probability Models.* New York: Holt, Rinehart and Winston.

[8] Bayramoglu, K.K. (2017). Reliability and mean residual life functions of coherent systems in an active redundancy. *Naval Research Logistics* **64**(1): 19–28.

[9] Chakraborty, S., & Pradhan, B. (2024). On cumulative residual extropy of coherent and mixed systems. *Annals of Operations Research* **340**(1): 59–81.

[10] Eryilmaz, S. (2013). On residual lifetime of coherent systems after the *r*th failure. *Statistical Papers* **54**(1): 243–250.

[11] Eryilmaz, S., & Bayramoglu, K. (2012). Residual lifetime of consecutive *k*-out-of-*n* systems under double monitoring. *IEEE Transactions on Reliability* **61**(3): 792–797.

[12] Feng, X., Zhang, S., & Li, X. (2013). A note on the mixture representation of the conditional residual lifetime of a coherent system. *Journal of Applied Probability* **50**(2): 475–485.

[13] Goli, S. (2019). On the conditional residual lifetime of coherent systems under double regularly checking. *Naval Research Logistics* **66**(4): 352–363.

[14] Goliforushani, S., Asadi, M., & Balakrishnan, N. (2012). On the residual and inactivity times of the components of used coherent systems. *Journal of Applied Probability* **49**(2): 385–404.

[15] Guo, Z., Zhang, J., & Yan, R. (2022). On inactivity times of failed components of coherent system under double monitoring. *Probability in the Engineering and Informational Sciences* **36**(3): 923–940.

[16] Jahanshahi, S.M.A., Zarei, H., & Khammar, A.H. (2020). On cumulative residual extropy. *Probability in the Engineering and Informational Sciences* **34**(4): 605–625.

[17] Jasiński, K. (2023). On the status of component failures in a working coherent system when the lifetimes are DNID random variables. *Statistics* **57**(1): 175–194.

[18] Khaledi, B.E., & Shaked, M. (2007). Ordering conditional lifetimes of coherent systems. *Journal of Statistical Planning and Inference* **137**(4): 1173–1184.

[19] Kharazmi, O., & Balakrishnan, N. (2023). Cumulative and relative cumulative residual information generating measures and associated properties. *Communications in Statistics-Theory and Methods* **52**(15): 5260–5273.

[20] Kochar, S., Mukerjee, H., & Samaniego, F.J. (1999). The "signature" of a coherent system and its application to comparison among systems. *Naval Research Logistics* **46**(5): 507–523.

[21] Lad, F., Sanfilippo, G., & Agro, G. (2015). Extropy: complementary dual of entropy. *Statistical Science* **30**(1): 40–58.

[22] Li, X., & Zhang, Z. (2008). Some stochastic comparisons of conditional coherent systems. *Applied Stochastic Models in Business and Industry* **24**(6): 541–549.

[23] Li, X., & Zhao, P. (2006). Some aging properties of the residual life of *k*-out-of-*n* systems. *IEEE Transactions on Reliability* **55**(3): 535–541.

[24] Li, X., & Zhao, P. (2008). Stochastic comparison on general inactivity time and general residual life of *k*-out-of-*n* systems. *Communications in Statistics – Simulation and Computation* **37**(5): 1005–1019.

[25] Marichal, J.L., & Mathonet, P. (2011). Extensions of system signatures to dependent lifetimes. *Journal of Multivariate Analysis* **102**(5): 931–955.

[26] Misra, N., & van der Meulen, E.C. (2003). On stochastic properties of *m*-spacings. *Journal of Statistical Planning and Inference* **115**(2): 683–697.

[27] Navarro, J. (2018a). Distribution-free comparisons of residual lifetimes of coherent systems based on copula properties. *Statistical Papers* **59**(2): 781–800.

[28] Navarro, J. (2018b). Stochastic comparisons of coherent systems. *Metrika* **81**(4): 465–482.

[29] Navarro, J., Balakrishnan, N., & Samaniego, F.J. (2008). Mixture representations of residual lifetimes of used systems. *Journal of Applied Probability* **45**(4): 1097–1112.

[30] Navarro, J., & Cali, C. (2018). Inactivity times of coherent systems with dependent components under periodical inspections. *Applied Stochastic Models in Business and Industry* **34**(1): 1–22.

Downloaded from https://www.cambridge.org/core. UNIVERSIDAD AUTONOMA METROPOLITANA, on 17 Nov 2026 at 01:28:28, subject to the Cambridge Core terms of use, available at https://www.cambridge.org/core/terms. https://doi.org/10.1017/S0269964826100369

[31] Navarro, J., & Durante, F. (2017). Copula-based representations for the reliability of the residual lifetimes of coherent systems with dependent components. *Journal of Multivariate Analysis* **158**: 87–102.
[32] Navarro, J., & Gomis, M.C. (2016). Comparisons in the mean residual life order of coherent systems with identically distributed components. *Applied Stochastic Models in Business and Industry* **32**(1): 33–47.
[33] Navarro, J., Pellerey, F., & Longobardi, M. (2017). Comparison results for inactivity times of k-out-of-n and general coherent systems with dependent components. *Test* **26**(4): 822–846.
[34] Navarro, J., & Rychlik, T. (2007). Reliability and expectation bounds for coherent systems with exchangeable components. *Journal of Multivariate Analysis* **98**(1): 102–113.
[35] Pakdaman, Z., & Alizadeh Noughabi, R. (2025a). A new representation of some extropy-related measures based on probability density quantile. *International Journal of Reliability, Quality and Safety Engineering* **32**(5): 2550013.
[36] Pakdaman, Z., & Alizadeh Noughabi, R. (2025c). Analyzing the cumulative residual extropy of system inactivity times and revealing system complexity. *Journal of Inequalities and Applications* **2025**(1): 117.
[37] Pakdaman, Z., & Alizadeh Noughabi, R. (2026a). Informational Complexity of Inactivity Times of the Failed Components through Cumulative Residual Extropy and Jensen Divergence. *International Journal of Reliability, Quality and Safety Engineering*.
[38] Pakdaman, Z., & Hashempour, M. (2021). Mixture representations of the extropy of conditional mixed systems and their information properties. *Iranian Journal of Science and Technology, Transactions A: Science* **45**(3): 1057–1064.
[39] Pakdaman, Z. Noughabi, R. A. (2026b). Extropy analysis of the inactivity times of the failed components in coherent systems with applications to estimation and image processing. *Scientific Reports*.
[40] Pakdaman, Z., & Noughabi, R.A. (2025b). On the study of the cumulative residual extropy of mixed used systems and their complexity. *Probability in the Engineering and Informational Sciences* **39**(1): 122–140.
[41] Pakdaman, Z., & Noughabi, R.A. (2026). Discovering the complexity of residual lifetimes of live components in the coherent system using cumulative residual extropy. *Probability in the Engineering and Informational Sciences* **40**(3): 1–31.
[42] Parvardeh, A., Balakrishnan, N., & Arshadipour, A. (2018). A note on the conditional residual lifetime of a coherent system under double monitoring. *Communications in Statistics – Theory and Methods* **47**(10): 2373–2378.
[43] Poursaeed, M.H. (2010). A note on the mean past and the mean residual life of a $(n - k + 1)$-out-of-n system under multi monitoring. *Statistical Papers* **51**(2): 409–419.
[44] Qiu, G., Wang, L., & Wang, X. (2019). On extropy properties of mixed systems. *Probability in the Engineering and Informational Sciences* **33**(3): 471–486.
[45] Samaniego, F.J. (1985). On closure of the IFR class under formation of coherent systems. *IEEE Transactions on Reliability* **34**(1): 69–72.
[46] Samaniego, F.J. (2007). *System Signatures and Their Applications in Engineering Reliability.* New York: Springer.
[47] Saranya, P., & Sunoj, S.M. (2024). On Relative Cumulative Extropy, Its Residual (Past) Measures and their Applications in Estimation and Testing. *Journal of the Indian Society for Probability and Statistics* **25**(1): 199–225.
[48] Shaked, M., & Shanthikumar, J.G. (2007). *Stochastic Orders.* New York: Springer.
[49] Shannon, C. (1948). A mathematical theory of communication. *The Bell System Technical Journal* **27**(3): 379–423.
[50] Sharifi, M., Taghipour, S., & Zaretalab, A. (2024). State-based transition probabilities for systems subject to periodic inspection interval. *Quality Technology & Quantitative Management* **21**(5): 633–655.
[51] Ucer, B., & Gurler, S. (2012). On the mean residual lifetime at system level in two-component parallel systems for the FGM distribution. *Journal of Mathematics and Statistics* **41**(1): 139–145.
[52] Zhang, Z., Du, X., Balakrishnan, N., & Yan, R.Y. (2026). Ordering and aging properties of surviving components in coherent systems. *Communications in Statistics-Theory and Methods* **55**(5): 1556–1567.
[53] Zhang, Z., & Meeker, W.Q. (2013). Mixture representations of reliability in coherent systems and preservation results under double monitoring. *Communications in Statistics – Theory and Methods* **42**(2): 385–397.
[54] Zhang, Z., & Yang, Y. (2010). Ordered properties on the residual life and inactivity time of $(n - k + 1)$-out-of-n systems under double monitoring. *Statistics & Probability Letters* **80**(9): 711–717.

Cite this article: Alizadeh Noughabi R. and Pakdaman Z. (2026). Inspection-conditioned uncertainty and complexity in coherent systems under double periodic inspections: extropy-based measures. *Probability in the Engineering and Informational Sciences* 1–44. https://doi.org/10.1017/S0269964826100369

Downloaded from https://www.cambridge.org/core. UNIVERSIDAD AUTONOMA METROPOLITANA, on 17 Nov 2026 at 01:28:28, subject to the Cambridge Core terms of use, available at https://www.cambridge.org/core/terms. https://doi.org/10.1017/S0269964826100369